AD-A185 035 INTERLAMINAR SHEAR FRACTURE TOUGHNESS AND FATIGUE THRESHOLDS FOR COMPOSIT.. (U) NATIONAL AERONAUTICS AND SPACE ADMINISTRATION HAMPTON VA LANG.. 1/1

UNCLASSIFIED T K O'BRIEN ET AL. AUG 87 NASA-TM-89137 F/G 11/2 NL

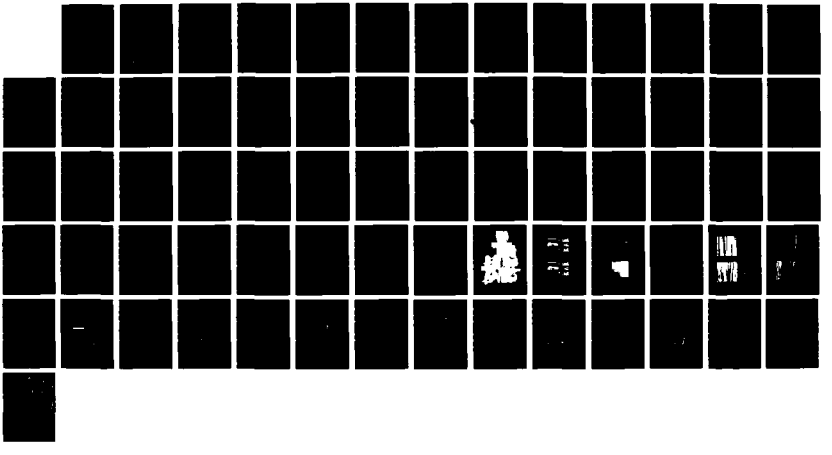

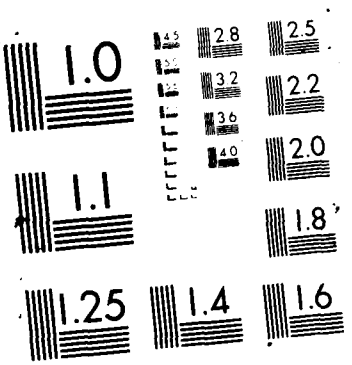
1.0
1.1
1.25
1.4
1.6
1.8
2.0
2.2
2.5
2.8
3.2
3.6
4.0

NASA TECHNICAL MEMORANDUM 89157

USAAVSCOM TECHNICAL MEMORANDUM 87-B-9

INTERLAMINAR SHEAR FRACTURE TOUGHNESS AND FATIGUE THRESHOLDS FOR COMPOSITE MATERIALS

T. KEVIN O'BRIEN, GRETCHEN B. MURRI, AND SATISH A. SALPEKAR

AUGUST 1987

NASA
National Aeronautics and Space Administration

Langley Research Center
Hampton, Virginia 23665

1. Report No. USAAVSCOM TM 87-B-9 NASA TM-89157	2. Government Accession No. AD-A185 855	3. Recipient's Catalog No.
4. Title and Subtitle INTELAMINAR SHEAR FRACTURE TOUGHNESS AND FATIGUE THRESHOLDS FOR COMPOSITE MATERIALS		5. Report Date August 1987 6. Performing Organization Code
7. Author(s) T. Kevin O'Brien, Gretchen B. Murri and Satish A. Salpekar		8. Performing Organization Report No. 10. Work Unit No. 505-63-01-05
9. Performing Organization Name and Address NASA Langley Research Center U.S. Army Aviation Research and Technology Activity (AVSCOM) Aerostructures Directorate Hampton, VA 23665-5225		11. Contract or Grant No.
12. Sponsoring Agency Name and Address National Aeronautics and Space Administration Washington, DC 20546 and U. S. Army Aviation Systems Command St. Louis, MO 63166		13. Type of Report and Period Covered Technical Memorandum 14. Army Project No. 1L161102AH45C

15. Supplementary Notes
T. Kevin O'Brien and Gretchen B. Murri, Langley Research Center, Hampton, VA
Satish A. Salpekar, Analytical Services & Materials, Inc., Hampton, VA

16. Abstract

Static and cyclic end-notched flexure (ENF) tests were conducted on a T300/BP907 graphite epoxy, an S2/SP250 glass epoxy, and an AS4/PEEK graphite thermoplastic to determine their interlaminar shear fracture toughness and fatigue thresholds for delamination in terms of limiting values of the mode II strain energy release rate, G_{II}, for delamination growth. The influence of precracking and data reduction schemes are discussed. Finite-element analysis indicated that the beam theory calculation for G_{II} with the transverse shear contribution included was reasonably accurate over the entire range of crack lengths. Cyclic loading significantly reduced the critical G_{II} for delamination. A threshold value of the maximum cyclic G_{II} below which no delamination occurred after one million cycles was identified for each material. In addition, residual static toughness tests were conducted on glass epoxy specimens that had undergone one million cycles without delamination. A linear mixed-mode delamination criteria was used to characterize the static toughness of several composite materials; however, a total G threshold criterion appears to characterize the fatigue delamination durability of composite materials with a wide range of static toughnesses.

17. Key Words (Suggested by Author(s)) Fatigue Delamination Interlaminar Shear Composite Materials	18. Distribution Statement Unclassified - Unlimited Subject Category 24		
19. Security Classif. (of this report) Unclassified	20. Security Classif. (of this page) Unclassified	21. No. of Pages 67	22. Price* A04

*For sale by the National Technical Information Service, Springfield, Virginia 22161

SUMMARY

Static and cyclic end-notched flexure (ENF) tests were conducted on three materials to determine their interlaminar shear fracture toughness and fatigue thresholds for delamination in terms of limiting values of the mode II strain energy release rate, G_{II}, for delamination growth. Data were generated for three different materials: a T300/BP907 graphite epoxy, an S2/SP250 glass epoxy, and an AS4/PEEK graphite thermoplastic. The influence of precracking and data reduction schemes on the mode II toughness and fatigue behavior are discussed. Finite element analysis indicated that the beam theory calculation for G_{II} with the transverse shear contribution included was reasonably accurate over the entire range of crack lengths. However, compliance measurements for the three materials tested, and the variation in compliance with crack length, differed from the beam theory predictions. For materials that exhibited linear load-deflection behavior, G_{IIc} values determined from compliance calibration measurements provided the most conservative and accurate estimate of the interlaminar shear fracture toughness. Cyclic loading significantly reduced the critical G_{II} for delamination. A threshold value of the maximum cyclic G_{II} below which no delamination occurred after one million cycles was identified for each material to quantify the degradation in interlaminar shear fracture toughness in fatigue. In addition, residual static toughness tests were conducted on glass epoxy specimens that had undergone one million cycles without delamination. These residual static tests, and the initial static tests on the tough AS4/PEEK graphite thermoplastic, exhibited nonlinear load-deflection behavior. For these cases, the load at deviation from nonlinearity was used to determine the interlaminar shear fracture toughness. A linear mixed-mode delamination criterion

was used to characterize the static toughness of several composite materials; however, a total G threshold criterion appears to be sufficient for characterizing the fatigue delamination durability of composite materials with a wide range of static toughnesses.

NOMENCLATURE

A_i	Parameters determined from fit of compliance calibration data (i=0,1,3)
a	Delamination Length
b	Beam width
C	Flexural compliance of ENF specimen
C_0	Flexural compliance of uncracked ENF specimen (a=0)
C_{SH}	Flexural compliance calculated from beam theory including the contribution of transverse shear
C^0_{SH}	Flexural compliance of uncracked ENF specimen (a=0) including the contribution of transverse shear
E_{11}	Axial modulus of lamina in fiber direction
E^{FX}_{11}	Axial modulus of lamina calculated from compliance measurement in three point bend test
E^{AX}_{11}	Axial modulus of lamina measured from tension test of ENF specimen
E_{22}	Modulus of a unidirectional lamina transverse to the fiber direction
G_{12}	In-plane shear modulus of a unidirectional lamina
G_{13}	Transverse shear modulus of a unidirectional lamina
G	Total strain energy release rate for delamination growth
G_c	Critical value of strain energy release rate for delamination onset

G_{th} Threshold maximum cyclic G for delamination onset in fatigue

G_I Strain energy release rate for delamination growth due to interlaminar tension, mode I

G_{Ic} Interlaminar tension fracture toughness

G_{II} Strain energy release rate for delamination growth due to interlaminar shear, mode II

G_{II}^{BT} Mode II strain energy release rate as calculated by beam theory

G_{II}^{SH} Mode II strain energy release rate calculated by beam theory with transverse shear contribution

G_{II}^{FE} Mode II strain energy release rate from finite element analysis

G_{IIc} Interlaminar shear fracture toughness

G_{IIc}^{CC} Critical mode II strain energy release rate at delamination onset calculated from compliance calibration measurements

G_{IIc}^{CCSH} Critical mode II strain energy release rate for delamination onset calculated from compliance calibration including transverse shear

G_{IIc}^{SC} Critical mode II strain energy release rate for subcritical delamination growth

G_{IIc}^{SCSH} Critical mode II strain energy release (including transverse shear) for subcritical delamination growth

G_{IIth} Threshold maximum cyclic G_{II} for delamination in fatigue

h Beam half-thickness

L Beam half-span

P Out-of-plane load

P_c Critical load at delamination onset

P_{NL} Load at onset of non-linear behavior

R Ratio of minimum to maximum cyclic load

x,y,z Cartesian coordinates

A-1

δ Center point out-of-plane displacement

δ_c Critical center point displacement at delamination onset

μ Coefficient of sliding friction for the delaminated ENF specimen

ν_{12} Poisson's ratio of a unidirectional lamina

INTRODUCTION

Delamination failures commonly occur in highly loaded composite structures. One of the predominant loads experienced by many composite structures is interlaminar shear. Several tests have been used to calculate interlaminar shear strength of composites, but all of them have severe limitations [1]. Perhaps the most popular of these tests is the short beam shear (SBS) test, which consists of a small unidirectional coupon loaded in three-point bending. Attempts have been made to generate interlaminar shear S-N curves for composite laminates using this SBS test [2]. However, short beam shear test specimens often fail in a mode different than interlaminar shear [3]. Furthermore, the interlaminar shear S-N data generated by the SBS test may not represent the generic material behavior, and hence, may not be applicable to composite structures of differing layups and thicknesses [4].

In order to assess the delamination durability of composites under cyclic loads, tests for interlaminar fracture toughness have been conducted to determine fatigue thresholds for delamination in terms of limiting values of the strain energy release rate, G, associated with delamination growth [5-8]. Because these fatigue thresholds are calculated in terms of G, they represent generic material behavior that is independent of the composite layup or geometry. The end-notched flexure (ENF) test was recently developed and evaluated for measuring the interlaminar shear fracture toughness, G_{IIc}, of composite materials [9-20]. This ENF test consists of a 24-ply unidirectional beam loaded in three-point bending (Fig.1). The specimen contains an insert at the mid-plane of one end to simulate an initial delamination. The crack tip is

extended beyond the front of the insert before loading to obtain a sharp crack tip. The load measured at the onset of delamination from the precrack is substituted into an analysis for G_{II} to calculate the interlaminar shear fracture toughness, G_{IIc}. In this study, several techniques previously proposed to calculate G_{II} were evaluated and compared.

In a previous study [12] the static ENF test was shown to be useful as a means of screening various materials for improved interlaminar shear fracture toughness. In this study, both static and cyclic flexural loading was applied to the beam to generate interlaminar shear fracture toughnesses, G_{IIc}, and fatigue thresholds, G_{IIth}, for glass-epoxy, graphite-epoxy, and graphite-thermoplastic materials. Cyclic loads were applied by means of a roller support fixture (fig.2). This fixture allows the specimen to rest on two pins or rollers, which are mounted on ball bearings, while the load is applied to the center of the specimen by another roller (fig. 3). Interlaminar shear fatigue thresholds were compared to G_c thresholds for mixed-mode delamination generated from cyclic edge delamination tests. A delamination fatigue failure criterion is proposed based on the delamination fatigue thresholds measured from a variety of interlaminar fracture toughness tests.

MATERIALS

Unidirectional panels with midplane inserts were manufactured and cut into ENF test specimens for three materials. Test specimens of S2/SP250 glass-epoxy were manufactured, from prepreg supplied by the 3M company, by Bell Helicopter Textron under NASA contract NAS1-18199. Test specimens of T300/BP907 graphite-epoxy were manufactured at NASA Langley from prepreg supplied by American Cyanamid. Test specimens of AS4/PEEK were cut from panels manufactured by

Imperial Chemical Industries. All test coupons were approximately six inches long by one inch wide and 24 plies thick. The average ply thicknesses for the T300/BP907, AS4/PEEK, and S2/SP250 were 0.0063, 0.0052, and 0.0095 inches, respectively. Table 1 lists material properties, average ENF specimen thicknesses, 2h, and fiber volume fraction, V_f, measured for the three materials. The axial modulus in the fiber direction, E_{11}, was measured from tension tests on the 24-ply ENF specimens. The transverse modulus, E_{22}, shear modulus, G_{12}, and Poisson's ratio, ν_{12}, were measured from 90°, ±45°, and 0° tension tests. The fiber volume fractions of the materials were calculated from the fiber areal weight of the prepreg divided by the product of the fiber density and the average ply thickness measured for the ENF test specimens. The crystalline percentage of the AS4/PEEK composites was 24%, as determined by wide angle X-ray scattering [11].

TEST PROCEDURES

Precracking

Previous studies have indicated that G_{IIc} values measured in the ENF test by propagating a crack from the insert, i.e. measured without a precrack, will increase with insert thickness [12]. Other studies have indicated that the lowest values of G_{IIc} were measured when a sharp precrack was grown from the insert before the bending load was applied [10,14-20]. In this study, three precracking techniques were used. The first technique was to clamp the specimen across the width slightly ahead of the insert, and then wedge the crack surfaces open until a sharp crack formed and grew to the clamp. This created a tension [illegible]. The second technique was to move the specimen in the three

point bend fixture so that the initial crack length was nearly equal to the half-span length, i.e., the end of the insert was close to the center roller. The specimen was then loaded in three point bending to propagate the crack from the end of the insert to a position under the center roller. This produced a shear (mode II) precrack. Then the specimen was positioned in the test fixture to the desired initial crack length and tested. The third technique was identical to the second except that the precrack was grown at a relatively high cyclic load, requiring relatively few load cycles, and then was repositioned and tested under a static load. The advantage of the last technique was that the straightness of the delamination front could be confirmed after the test by examining the fracture surfaces.

As will be shown later, the static shear precrack was used to generate the majority of the test data. By using this approach, the G_{IIc} and cyclic G_{th} values obtained were representative of the interlaminar shear fracture toughness, and fatigue threshold for delamination growth, due to interlaminar shear stresses at the tip of a delamination that was created by large interlaminar shear stresses. These large shear stresses could have developed during a high load that the structure experienced during its lifetime. Previous work on composite fatigue suggests that it is the high loads in the spectrum that are the most damaging in terms of creating delaminations, and subsequent reductions in residual strength and life. Therefore, the common practice used for metals of coaxing a precrack by applying blocks of low cyclic loads over many cycles was not adopted. The tension precrack was not used, even though it may yield slightly more conservative values of G_{IIc}, because it was assumed that if a pure shear stress state existed at the delamination front, then the stress state in the material that created the delamination must have also been pure shear.

Crack Length Determination

To locate the crack, the sides of the graphite composites were painted white with water-soluble typewriter correction fluid. The glass composites were translucent, and therefore did not require an enhancement of the edge to locate the crack tip. Figure 3 shows the graphite and glass composites as they appeared when loaded in the three point bend apparatus. The initial crack length was measured from the centerline of the right-hand roller to the end of the crack before testing. The average of the crack length measurements from both specimen edges was used in the data reduction to minimize error associated with an uneven precrack. This crack length measurement could sometimes be verified after the test by splitting the laminate into two pieces and observing the difference between the precrack fracture surface and the fracture surface caused by the three point bending. For example, figure 4 shows the change in fracture surface appearance for two AS4/PEEK composites that either had a static mode II precrack and was then cycled in mode II, or had a cyclic mode II precrack and was then loaded statically in mode II. The static and cyclic shear fracture surfaces have markedly different appearances, which allows an accurate determination of initial crack length from the end of the precrack to the imprint of the support pin on the outer surface.

Static Tests

Precracked ENF specimens were positioned in the three-point bending fixture to the desired initial crack length. The fixture had 0.25-in. diameter steel rods, supported by annular ball bearings encased in aluminum channels at

each end, that applied the loads across the specimen width. In addition, the fixture had a degree of freedom out of the plane of the test specimen due to additional pinned joints between the cross heads and the rollers. This extra degree of freedom assured uniform loading across the width of the laminate for all three rollers. This combination of loading pins and annular ball bearings created a frictionless roller system ensuring simple support conditions for both static and cyclic loading. However, because the ENF specimen was precracked on one side only, the deformation was asymmetric under the applied loading. Hence, small side forces could develop causing the specimen to shift on the rollers during the test. To prevent this from occurring, a small restraining bar was attached to the fixture at the uncracked end of the specimen (fig.2-3). This restraining bar was free to move with the specimen as it deflected.

All tests were conducted with a span length of three inches, i.e. L=1.5 inches in fig.1. Loads were applied using a servo-hydraulic test stand in stroke control at a rate of 0.1 in./min. until the delamination grew. The delamination grew to a point immediately under the center load point for most crack lengths tested. Some specimens were repositioned to a new crack length to yield additional toughness values from the same specimen. Center point displacements were measured with a direct current differential transducer (DCDT) whose rod was supported by a spring as shown in figures 2-3. The load-displacement behavior of the specimen and applied load versus machine stroke were plotted on an x-y-y' recorder. Typical load-displacement results for the three materials tested are shown in figure 5. The load-displacement plots were linear for the glass-epoxy laminates, slightly non-linear for the graphite-epoxy laminates, and significantly non-linear for the graphite-thermoplastic laminates.

Fatigue Tests

Precracked ENF specimens were positioned in the three point bend apparatus to the desired initial crack length. Specimens were loaded statically in stroke control to the mean load, and then cycled sinusoidally at a frequency of 5 Hz. at a maximum constant load amplitude corresponding to an R ratio of 0.1. Specimens were cycled until the onset of stable delamination growth was detected by a combination of visual observation and a drop off in the cyclic load at a constant cyclic stroke. The number of cycles to delamination onset was recorded, and the specimen was reloaded to the mean load to record the compliance at the new crack length.

Residual Static Tests

Several S2/SP250 glass-epoxy laminates were tested statically after undergoing 10^6 or more cycles at low cyclic loads below the threshold for delamination growth. The procedure used for these tests was identical to the procedure used for the initial static tests. The load-displacement plots were nonlinear for these residual static tests, similar to the initial static tests on AS4/PEEK.

Compliance Calibration

Two precracked ENF specimens of each material were placed in the three-point-bend apparatus repeatedly, to simulate crack lengths ranging from a=0 to a=L, by shifting the position of the specimen in the three point bending

apparatus and thereby changing the distance between the right end roller and the delamination front. At each unique delamination length position, the specimen was loaded high enough to obtain a load-deflection plot but without extending the delamination. The slopes of the load-deflection plots were measured to obtain a record of specimen compliance as a function of crack length.

ANALYSIS

Several techniques have been proposed for calculating G_{II} in the ENF specimen. In this section, these techniques will be outlined and compared. In subsequent sections, the ENF test data will be reduced using several of these methods and compared. Finally, based on the observations from this study, particular data reduction techniques will be recommended.

Beam Theory

Figure 1 shows the ENF specimen configuration where L is the half-span length, 2h is the laminate thickness, b is the laminate width, P is the applied load, and a is the initial delamination length as defined by the distance between the load support and the delamination front. A closed-form equation for the strain energy release rate associated with delamination growth due to interlaminar shear was derived in reference [9] for this test using linear beam theory. This analysis yielded

$$G_{II}^{BT} = \frac{9\ P^2\ a^2\ C}{2b(2L^3 + 3a^3)} \qquad (1)$$

where C is the flexural compliance defined as the ratio of the center point deflection, δ, to the applied load, P, and derived from the linear beam theory as

$$C = \frac{2L^3 + 3a^3}{8E_{11}bh^3} = \frac{\delta}{P} \qquad (2)$$

Substituting eq.(2) into eq.(1) yields the following equation for G_{II} in terms of the axial modulus, E_{11}

$$G_{II}^{BT} = \frac{9P^2\ a^2}{16E_{11}b^2h^3} \qquad (3)$$

Transverse Shear and Friction Contribution

The beam theory equations may be modified to include the influence of transverse shear deformation [14] where

$$C_{SH} = \frac{2L^3 + 3a^3}{8E_{11}bh^3}\left(1 + \frac{2(1.2L + 0.9a)h^2E_{11}}{(2L^3 + 3a^3)\ G_{13}}\right) \qquad (4)$$

$$G_{II}^{SH} = \frac{9\,P^2\,a^2\,C}{2b(2L^3 + 3a^3)}\left(1 + 0.2(E_{11}/G_{13})(h/a)^2\right) \qquad (5)$$

For transversely isotropic materials, the transverse shear modulus, G_{13}, is assumed to be equal to the inplane shear modulus, G_{12}. For shear compliant materials where E_{11}/G_{13} is high, or for thick beams, the contribution of the shear deformation terms may be significant. Also, eq.(5) indicates that for any material and span length, the contribution of transverse shear will be the greatest for the shorter crack lengths.

The contribution of friction to crack growth retardation has been estimated previously [14]. Friction decreases the energy available for crack propagation such that

$$G_{II}(\mu) = G_{II}^{SH} - \frac{3P^2\mu\,a}{4E_{11}b^2h^2} \qquad (6)$$

where μ is the coefficient of sliding friction for the fracture surface. For reasonable values of μ, the reduction in G_{IIc} after including the friction contribution was found to be only 2 to 5% for graphite composites with typical test coupon geometries [14]. No attempt was made in this study to quantify μ or its influence on G_{II}.

Compliance Calibration Method

An alternate method for determining G_{IIc} is the use of a compliance calibration curve. An experimental curve of normalized compliance, C/C_0 (where C is the compliance as measured by beam theory (eq.2) and C_0 is the compliance for the beam with no crack) versus normalized crack length cubed, $(a/L)^3$, can be

constructed using the technique described earlier. A linear regression fit of the data yields

$$C/C_0 = A_0 + A_3(a/L)^3 \tag{7}$$

where A_3 is the slope of the line fit to the data and A_0 is the y-intercept. The linear beam theory would yield A_0=1 and A_3=1.5. G_{IIc} by this approach is obtained by differentiation of C in eq.(7) with respect to a, and multiplication by $P_c^2/2b$, yielding

$$G_{IIc}^{CC} = \frac{3A_3P_c^2a^2C_0}{2bL^3} \tag{8}$$

A similar compliance calibration technique may be employed by rearranging eq.(4) for beam compliance with transverse shear such that

$$C_{SH} = \frac{2L^3}{8E_{11}bh^3}\left(1 + 1.2\gamma + 0.9\gamma(a/L) + 1.5(a/L)^3\right) \tag{9}$$

where $\gamma = (h/L)^2(E_{11}/G_{13})$, and the compliance of an uncracked beam is

$$C_{SH}^0 = \frac{2L^3}{8E_{11}bh^3}\left(1 + 1.2\gamma\right) \tag{10}$$

Dividing eq.9 by eq.10 yields

$$C_{SH}/C_{SH}^0 = A_0 + A_1(a/L) + A_3(a/L)^3 \tag{11}$$

The beam theory with transverse shear would yield A_0=1, A_1=0.9Y/(1+1.2Y), and A_3=1.5/(1+1.2Y). These coefficients may also be determined independently from a least squares fit of the compliance versus crack length data. Differentiating eq(11) with respect to a, and multiplying by $P_c^2/2b$ yields

$$G_{IIc}^{CCSH} = \frac{P_c^2 C^0_{SH}}{2bL} \left(A_1 + 3A_3(a/L)^2 \right) \qquad (12)$$

Influence of nonlinear behavior

In references [16,18-20], deviations from the linear load-displacement curve for toughened matrix composites (such as the AS4/PEEK graphite-thermoplastic) in the ENF fracture test were attributed to the onset of subcritical crack growth and inelastic shear response of the material in the crack tip region. Scanning electron microscope photographs indicate that interlaminar shear fracture consists of the formation of matrix cracks at 45° to the original crack followed by a coalescence of these matrix cracks for extension of the delamination. In brittle matrix composites, such as the T300/5208 shown in fig.6, there is very little matrix yielding and the formation and coalescence of these cracks occurs simultaneously. Hence, the load-displacement record is linear. However, in tough matrix composites, such as the AS4/PEEK shown in fig.7, significant matrix yielding occurs during the formation and coalescence of these matrix cracks. Furthermore, these two events do not necessarily occur simultaneously, and the load-displacement record is non-linear.

One conservative approach is to estimate the mode II interlaminar fracture toughness using the load, P_{NL}, at which non-linear response is first observed. In this way, G_{IIc} may be thought of as a strain energy release rate parameter

for subcritical crack growth. In ref.[16,18-20], G_{IIc}^{SC} was evaluated by substituting the initial linear compliance, C, and the load at onset of nonlinear behavior, P_{NL}, in the strain energy release rate calculation of eq.(1) yielding

$$G_{IIc}^{SC} = \frac{9\, P_{NL}^2 a^2 C}{2b(2L^3 + 3a^3)} \tag{13}$$

Similarly, this subcritical fracture toughness may be estimated by using P_{NL} in eq(5) to include the contribution of transverse shear, or in eqs(8 & 12) to incorporate the compliance calibration information.

Finite Element Analysis

Finite element analyses of the ENF specimen have been performed to evaluate the strain energy release rate for delamination growth [13,15,18,20]. In ref.[13], a two-dimensional plane strain model using 1000 four-noded isoparametric elements with 2400 degrees of freedom was used to model the ENF specimen. The virtual crack closure technique was used to calculate G_{II} [22]. The element size in the vicinity of the crack was 0.02 by 0.02 mm (0.00079 by 0.00079 in). A nodal coupling technique implementing multi-point constraints was used to prevent overlapping of crack surfaces. In addition to the frictionless case, assumed coefficients of friction were used to estimate friction forces at nodes located on the crack surfaces. The ratio of G_{II}^{FE}/G_{II}^{BT} was plotted as a function of normalized crack length, a/L, for two graphite-epoxy ENF specimens with two different span lengths subjected to the same applied load. The results indicated that the deviation in G_{II} between the finite element analysis and beam

theory was significant at the shorter crack lengths ($a/L \leq 0.3$). However, if G_{II}^{FE}/G_{II}^{SH} is plotted, the agreement is fairly good over the entire range of crack lengths (fig.8).

In ref.[15,18,20], a two-dimensional plane stress analysis using four-noded isoparametric elements with Gauss numerical integration of order two was used with the virtual crack extension technique to calculate G_{II} for the ENF specimen. Elements at the crack tip had dimensions of 0.0127 by 0.0127 mm (0.0005 by 0.0005 in). The frictionless contact problem was incorporated in the analysis by connecting duplicate nodes across the crack interface with non-linear truss elements with zero tensile stiffness and infinite compression stiffness. The finite element results indicated that although the beam theory expressions for compliance were accurate, the beam theory expressions for G_{II} in eqs.(1,3,5) may be conservative by 10 to 48%, with the greatest deviation from beam theory occurring at $a/L \geq 0.4$. Further finite element results were generated for a wide range of crack lengths in ref.[20]. As indicated in fig.8, these results also showed that the finite element values of G_{II} diverged from the beam theory results for delamination lengths greater than 0.4L.

Recently, a two-dimensional plane strain finite element analysis was performed to verify if either one of the previous analyses, that yielded contradictory results, was valid [23]. The ENF specimen was modeled using eight-noded, isoparametric elements. The laminate modeled consisted of 24 plies, each having a ply thickness of 0.0056 inches. The span length was three inches, i.e., L=1.5 in. Material properties typical of a graphite thermoplastic composite were used

E_{11} = 15.7 Msi

E_{22} = 1.40 Msi

$$G_{12} = G_{13} = 0.65 \text{ Msi}$$

$$\nu_{12} = 0.3$$

Figure 9 shows a plot of a typical mesh. Three mesh refinements were performed by subdividing the square elements at the delamination front into four smaller square elements of equal size. The element size at the delamination front was 0.1905, 0.0953, and 0.0476 mm (0.0075, 0.00375, and 0.001875 inches) for the coarse, medium, and fine meshes, respectively. The element size was gradually increased away from the delamination front in both directions. The coarse, medium, and fine meshes had 312, 410, and 516 elements respectively.

Initially, the delaminated surfaces were allowed to deform freely. Results indicated that the delaminated surfaces would cross into one another, which is physically impossible. Therefore, the nodes along the delamination front were constrained to move the same distance in the vertical direction using multi-point constraints. Various a/L ratios between 0.2 and 0.9 were modeled in the analysis. This was achieved by shifting the supports and the central load point by the same amount along the mesh, which is analagous to shifting the beam in the three-point test fixture to test different crack lengths, as was done in the compliance calibration testing. The crack tip always remained between the central load and the near end support. Compliance values corresponding to the measured center-point displacement for a unit central load were calculated for the three meshes. Compliance values converged as the element size decreased from the coarse to the fine mesh. The G_{II} values were calculated using the virtual crack extension method. These G_{II} values also converged as the element size decreased from the coarse to the fine mesh. Furthermore, G_{II} values calculated using the global change in compliance agreed with the G_{II} values calculated using the local virtual crack closure technique.

Figure 10 shows G_{II}/P^2 as a function of a/L for the ENF specimen. Good agreement was observed between the G_{II}^{FE} values and the G_{II}^{SH} values calculated using eq.(5). A maximum deviation of 6.7% was observed for a/L = 0.4 (fig.8). A plane stress analysis was also performed at this crack length using the coarse mesh. The difference in the plane strain and plane stress values for G_{II} was only 0.79%. Hence, eq.(5) yields G_{II}^{SH} values that are reasonably accurate, although slightly conservative compared to the finite element results. The small reduction (between 2% and 5%) in G_{II} attributed to friction on the delaminated surfaces [14] may eliminate some of this difference. For example, by assuming that

$$G_{II}^{SH} \tilde{=} G_{II}^{FE} - \frac{3P^2 \mu a}{4E_{11} b^2 h^2} \qquad (14)$$

then G_{II}^{SH} calculated by eq.(5) may represent an accurate value of the mode II strain energy release rate. Hence, G_{II}^{SH} values represent reasonably accurate calculations of the strain energy release rate over a large range of a/L values in the ENF test.

RESULTS

Compliance Calibration

Compliance calibration curves were generated for all three materials tested. Specimen compliance was defined as the ratio of the center point deflection to the out-of-plane load. Center point deflection was measured by the DCDT mounted under the specimen (fig.2-3). Compliance was measured from the

slope of the load-deflection plot for each crack length tested. The compliance calculated using the DCDT-measured deflection was less than the compliance calculated using the stroke of the hydraulic ram. Hence, because the compliance used to calculate G_{II} was always calculated using the center point deflection measured directly from the DCDT, no correction for machine compliance was necessary. Compliance was measured for delamination lengths from a=0 to a=1.5 inches in increments of 0.1 inches.

The average of the two crack lengths measured from both edges was used to reduce the compliance calibration data. Furthermore, because calculation of the slope is very sensitive to errors in crack length measurement, the specimens used for compliance calibration tests were split apart and the edge measurements were examined for crack front deviation through the width. A distinct crack front was visible on the fracture surfaces at the transition from the shear precrack to the tensile fracture surface created by splitting the tested beam into two pieces. Both of the glass epoxy laminates had relatively straight delamination fronts. The T300/BP907 laminates had a deviation in delamination lengths between the two edges of 0.20 and 0.16 inches. One of the AS4/PEEK laminates had a deviation in delamination lengths between the two edges of 0.15 inches and the other laminate had a straight delamination front.

Two specimens of each material were used to generate compliance calibration data. Data were fit to eq.(7) using a linear least-squares regression analysis. Figure 11 shows the data and the linear fit to eq.(7) for one specimen of each of the three materials. Table 2 lists the values of the slope, A_3, the y-intercept, A_0, and the goodness of fit, r^2, calculated for each test of the three materials. If the beam theory is accurate, the slope should be 1.5, and the y-intercept should be 1. Of the three materials tested, only the AS4/PEEK

material had a slope close to 1.5. The T300/BP907 and the S2/SP250 had slopes that were significantly less than 1.5.

These same data were fit to eq(11) to determine the coefficients A_0, A_1, and A_3 in the cubic polynomial representation for the compliance of the ENF specimen with transverse shear incorporated. Table 3 lists the values of these parameters as determined by the least squares regression analysis. Also listed in table 3 are values for A_0, A_1, and A_3, calculated from beam theory with transverse shear using properties from table 1. As noted earlier in the linear regression analysis, the A_3 coefficient of the $(a/L)^3$ term is less than anticipated based on beam theory with transverse shear for the two epoxy materials. The additional A_1 coefficient of the linear (a/L) term, that was not present in the linear regression analysis, also appears in eq(12) for G_{II}. Table 3 shows that these values were also different from those calculated using beam theory.

In order to determine the contribution of the roller test fixture compliance to C, calibration tests were performed on the same specimens using a rigid knife edge support fixture described in ref.[12]. Table 2 lists the values of A_0, A_3, and r^2 determined from these tests. For the epoxy matrix materials, the slope, A_3, was closer to the beam theory value of 1.5 for tests conducted on the more rigid knife edge fixtures. The difference in slope calculated for the two fixtures was small for the graphite-epoxy (T300/BP907), however, the difference was significant for the glass/epoxy (S2/SP250). For the graphite/thermoplastic (AS4/PEEK), which showed the best agreement with the beam theory using the roller fixture, the slope calculated using the knife edge supports exceeded the beam theory value.

As a further check of the beam theory, the axial moduli of the compliance calibration specimens were measured in a uniaxial tension test using a one inch

long extensometer as described in reference [12]. These E_{11}^{AX} measurements were compared to E_{11}^{FX} values calculated from compliance measurements using eq.(2) where

$$E_{11}^{FX} = \frac{1 + 1.5(a/L)^3}{4b(h/L)^3 C} \qquad (15)$$

The E_{11}^{FX} values were calculated from compliance measurements for each crack length, measured in 0.1-inch increments, from 0 to 1.5 inches. As shown in fig. 12, E_{11}^{FX} values increased slightly at the longer crack lengths. An average value of E_{11}^{FX} over the range of crack lengths was calculated for each specimen. Table 4 compares the various measurements of E_{11}. The E_{11}^{FX} values were considerably less than the E_{11}^{AX} values, with the more compliant roller fixture yielding the lowest values. Table 5 lists the difference in the E_{11}^{FX} and E_{11}^{AX} values for the three materials. The graphite composites had over twenty percent difference in measured and calculated axial stiffness. If the transverse shear correction is included in the flexural compliance (eq. 4), then the estimate of E_{11}^{FX} becomes

$$E_{11}^{FX} = \frac{1 + 1.5\,(a/L)^3}{4b(h/L)^3 C - (h/L)^2[1.2 + 0.9(a/L)] / G_{13}} \qquad (16)$$

The second term in the denominator reflects the contribution of transverse shear. Hence, including transverse shear increases E_{11}^{FX}, but only by 4-5%. Therefore, the ENF specimens are not behaving as the beam theory would predict, even after the influence of transverse shear and test fixture compliance are included.

Examination of the specimen edges in an optical microscope indicated that the outermost three layers were thicker than the interior plies. This may result

from resin bleeding from the interior to the top and bottom surfaces during cure. This resulting inhomogeneity yields surface plies that are thicker, more resin rich, and hence, less stiff than the interior plies. When the laminate is loaded in bending, the specimen appears to be much less stiff than when it is loaded in tension, since the outermost plies carry the majority of the load in bending. Furthermore, this effect will be slightly different in the cracked and uncracked portion of the ENF specimens, resulting in a change in compliance with crack length that differs from the beam theory predictions. When this occurs, as evidenced by A_3 coefficients that are less than predicted by the beam theory (tables 2&3), the compliance calibration method should be used to reduce the data.

Static Tests

Tables 6-8 list the load at delamination onset, P_c, delamination length, a, compliance, C, and critical values of G_{II} using the various data reduction schemes for the T300/BP907, AS4/PEEK, and S2/SP250 laminates, respectively. These data are summarized in fig.13. Critical values of G_{II} were calculated using the measured compliance, crack length, and load at onset of delamination, P_c, in the beam theory eq.(1). The contribution of transverse shear was calculated using E_{11}, G_{13}, and h from table 1 in eq.(5). For all three materials, G_{IIc}^{SH} values were slightly greater than G_{IIc}^{BT} values, reflecting the small contribution of transverse shear. Initial compliance values for the uncracked beam, C_0, were calculated from eq(7) for each specimen tested using the measured compliance and crack length along with the coefficients A_3 and A_0, calculated using the roller fixtures in table 2. Then, G_{IIc}^{CC} and G_{IIc}^{CCSH} values were calculated from eqs(8 & 12) using appropriate coefficients from tables 2&3.

For all three materials, G_{IIc}^{CC} values were lower, and hence more conservative, than the beam theory values calculated with or without transverse shear. The largest differences occurred for the materials whose slope, A_3, deviated the greatest from the beam theory slope of 1.5 in eq. 7 (table 2).

Table 6 lists results for T300/BP907 graphite-epoxy. As noted earlier, the G_{IIc}^{CC} values yielded the lowest, i.e. the most conservative, estimate of toughness. The G_{IIc}^{CCSH} values were slightly different, indicating the small contribution due to transverse shear. The three tests run without precracks, where the delamination was initiated at the insert, yielded the highest apparent toughness. Because these delaminations started in the resin-rich pocket at the tip of the insert, they were not considered to be representative of naturally occurring delaminations. The tension precracked specimen yielded slightly lower toughness than the two shear precracked specimens. However, because these specimens had experienced large tensile deformations at the crack tip, they were also not considered to be representative of a naturally occurring delamination in a region of high shear stresses. Therefore, all remaining tests for the three materials were run on specimens that were precracked in shear, either statically or cyclically, to obtain a realistic interlaminar shear fracture toughness of the delaminated composite with shear deformation at the crack tip.

Table 7 lists results for AS4/PEEK graphite-thermoplastic. As shown in fig.13, there was a significant degree of scatter in the data from these nine tests. This scatter could be reduced if the high and low data points were discarded leaving only seven data points. As noted earlier, the G_{IIc}^{CC} values yielded lower, i.e. more conservative, estimates of toughness than the beam theory values, with or without transverse shear (table 7). However, the AS4/PEEK specimens exhibited significant nonlinear load-displacement behavior before unstable delamination growth. Therefore, both the beam theory and the compliance

calibration methods do not reflect the change in energy with crack growth that occurs after the compliance has increased at loads above P_{NL}. However, if subcritical crack growth is assumed to occur at the onset of nonlinearity, then eq.(14) may yield a more accurate representation of the interlaminar shear fracture toughness than eq.(11). Therefore, P_{NL} was used in the compliance calibration equations (11) to calculate the critical value of G_{II} for onset of subcritical delamination growth. Calculated values of G_{IIc}^{SC} and G_{IIc}^{SCSH} for the AS4/PEEK specimens tested are listed in table 7. These values calculated using the load at onset of nonlinear behavior, P_{NL}, are significantly lower than toughness values calculated using the critical load at unstable delamination growth, P_c. Interestingly, specimen #7 had the highest P_c, and hence the highest value of G_{IIc}^{CC}, but it had the lowest P_{NL}, thus yielding a relatively low value of G_{IIc}^{SC}. The two specimens that were precracked under cyclic shear loading, using a relatively high maximum load and a low number of cycles, had similar toughness values as the rest of the specimens that were precracked under static shear loads.

Table 8 lists results for the S2/3501-6 glass-epoxy. As noted earlier, the G_{IIc}^{CC} values yielded the lowest, i.e. the most conservative, estimate of toughness. In addition to the static tests, residual toughness tests were conducted on four specimens that had been subjected to relatively low maximum cyclic loads for at least one million fatigue cycles without delamination growth. These residual toughness values (Table 9) were consistently lower than the static toughness values (Table 8). Furthermore, these tests exhibited significant nonlinearity, similar to the behavior of the AS4/PEEK static tests. Therefore, eqs. (8) and (12) using P_{NL} were used to calculate G_{IIc}^{SC} and G_{IIc}^{SCSH} for these specimens (Table 9). As noted earlier for the AS4/PEEK material, the G_{IIc}^{SC} were lower than the G_{IIc}^{CC} values.

Fatigue Tests

Tables 10-12 list the cycles to delamination onset, N, maximum cyclic load, P_{max}, delamination length, a, compliance, C, and maximum cyclic G_{II} values using the various data reduction schemes for the T300/BP907, S2/SP250, and AS4/PEEK laminates, respectively. Figures 14-16 show the numbers of cycles to delamination onset as a function of maximum cyclic G_{II}^{CC} level for the three materials tested. All three materials exhibit significant reductions in critical G_{II} values for delamination onset with fatigue cycles, with an apparent threshold value for delamination onset in fatigue as indicated by the plateaus in figures 14-16. Hence, cyclic loading significantly reduces the critical G_{II} for delamination onset. These threshold values of G_{II} may be compared to G_{IIc} using the ENF test to quantify the degradation in interlaminar shear fracture toughness due to fatigue.

DISCUSSION

Compliance Calibration

Ideally, G_{IIc}^{CC} and G_{IIc}^{CCSH} values for each specimen should be determined using values of the A_3 and A_1 coefficients measured for each specimen. However, this would be very time consuming. Therefore, all the data were reduced using the average value of these coefficients calculated from the two compliance calibration tests for each material listed in tables (2&3), and C_0 was determined from eq(7) using the measured values of C and a for the particular test. An alternative would be to measure C_0 directly for each specimen, while

still using the average coefficients from just a few compliance calibration tests.

Static Tests

Because the compliance calibration values are the most conservative for materials that exhibit linear load-displacement behavior, and because they represent the actual change in compliance with delamination growth for the specimens tested, the interlaminar shear fracture toughness is best represented by G_{IIc}^{CC}. However, for materials that exhibit nonlinear load-displacement behavior, as was observed in the AS4/PEEK static tests or in the residual static tests on the S2/SP250 following high cycle fatigue, the interlaminar shear fracture toughness is characterized most conservatively by G_{IIc}^{SC} values. Because the growth of a mode II delamination actually corresponds to the coalescence of small tensile cracks oriented at 45° to the delamination plane in the resin layer between the plies, then mode II crack growth may be more stable if the resin toughness is high, or if the material at the delamination front has been cyclically deformed. Hence, the critical G_{II} for onset of subcritical (i.e. stable) delamination growth may provide a better, and more conservative, measure of the interlaminar shear fracture toughness in these cases.

Fatigue Tests

The ENF tests conducted in this study showed a significant, in some cases an order of magnitude, reduction in the mode II delamination durability of the three materials studied compared to their static interlaminar shear fracture toughnesses (fig.14-16). This reduction in delamination resistance during cyclic

loading was also observed in studies conducted using mixed-mode edge delamination tension tests [5-8]. Figure 17 shows the reduction in critical total G for delamination onset for two edge delamination tension (EDT) layups of T300/BP907 [7]. The two layups have intermediate and low percentages of mode II, with the remainder mode I. Also shown in figure 17 are the critical G_{II}^{CC} values for delamination onset (fig. 14) for static loading and for fatigue (with the same frequency and R-ratio as the EDT tests). The static G_c values are different for the three tests, with the layups having the highest percentage of G_{II} showing the largest apparent toughness. However, the G_{th} values are nearly identical for the two edge delamination layups and the ENF specimens. Hence, the static toughness of this material will vary with the ratio of mode I and II at the delamination front, but the fatigue threshold depends only on the total G, independent of the mode ratio.

Figure 18 shows the reduction in critical total G for delamination onset for a $(35_2/-35_2/0_2/90_2)_s$ edge delamination tension (EDT) layup of AS4/PEEK [8]. The total G for this layup consists predominantly of tension, G_I, with only a small shear component, G_{II}. Also shown in figure 18 are the critical G_{II} values from the ENF test for delamination onset in fatigue (fig. 16) under the same frequency and R-ratio. Although these two tests are different in that one consists of pure interlaminar shear and the other is predominantly interlaminar tension, the G_{th} values are nearly identical. Hence, as was noted earlier for the T300/BP907 material, the fatigue threshold for the AS4/PEEK appears to depend only on the total G, independent of the mode ratio.

Previously a linear delamination failure criterion was proposed for delamination failure under static loads [24]. This criterion had the form

$$\frac{G_I}{G_{Ic}} + \frac{G_{II}}{G_{IIc}} = 1 \qquad (17)$$

Figure 19 from reference 24 shows interlaminar fracture toughness data plotted from the literature for materials with matrices ranging from very brittle to very tough. Pure mode I data (G_{Ic} values) were generated using double cantilever beam (DCB) specimens and are plotted on the ordinate. Pure mode II data (G_{IIc} values) were generated using ENF specimens and are shown on the abscissa. Mixed mode data (G_c values) were generated using edge delamination tension (EDT) and crack lap shear (CLS) specimens, and are plotted at the appropriate coordinates according to the G_I and G_{II} component for each test. For all the materials, the data fit the linear criterion given by eq.(17). However, for the brittle materials, like the epoxy matrix materials in this study, $G_{Ic} << G_{IIc}$; whereas for the toughened matrix materials, such as AS4/PEEK, G_{Ic} was nearly equal to G_{IIc}. Therefore, for the toughened matrix materials, noting that $G = G_I + G_{II}$ and that $G_{Ic} = G_{IIc}$, eq.(17) reduces to

$$G = G_c \tag{18}$$

A linear failure criterion similar to eq.(17) may be assumed for delamination onset under cyclic loading as

$$\frac{G_I}{G_{Ith}} + \frac{G_{II}}{G_{IIth}} = 1 \tag{19}$$

However, as indicated in figures 17 and 18, the threshold value for delamination onset in fatigue appears to be independent of mode ratio, even for the brittle epoxy matrix materials where the static toughness is dependent on mode ratio.

Fig. 20 shows the static and fatigue delamination strain energy release rate data for T300/BP907. Linear failure criteria are plotted for the static interlaminar fracture toughness and fatigue threshold between the predominantly

mode I (EDT) and mode II (ENF) toughness values. The fatigue envelope is lower than the static envelope, with the greatest apparent reduction occurring for the pure mode II tests as indicated in figure 17. The static envelope is skewed because $G_{Ic} << G_{IIc}$, whereas the fatigue envelope approaches a 45° line reflecting the near equality of the threshold values of G_I and G_{II}. Therefore, for the brittle epoxy matrix composites, the fatigue delamination criterion of eq.(19) simply reduces to

$$G_{max} = G_{th} \tag{20}$$

Fig. 21 shows the static and fatigue delamination strain energy release rate data for AS4/PEEK. Linear failure criteria are plotted for the static interlaminar fracture toughness and fatigue threshold between the predominantly mode I (EDT) and mode II (ENF) toughness values. The fatigue envelope is lower than the static envelope, with the greatest apparent reduction occurring in pure mode II tests. The static envelope is skewed because $G_{Ic} << G_{IIc}^{SC}$, whereas the fatigue envelope approaches a 45° line reflecting the near equality of the threshold values of G_I and G_{II}. Therefore, the fatigue delamination criterion of eq.(20) may apply for the tough AS4/PEEK composite as well as for the epoxy matrix composites. However, several inconsistencies in AS4/PEEK data have been noted in the literature [8]. This may be illustrated by comparing the data in figures 19 and 21. The static toughness data for PEEK composites shown in fig.19 indicate that a total G criterion should apply for this material, i.e., $G_{Ic} = G_{IIc}$. However, the data in fig. 21 indicates that $G_{Ic} < G_{IIc}$. The G_{IIc} value in fig. 19 was calculated using ENF specimens that exhibited unstable propagation from a tensile precrack. This value is similar to the G_{IIc}^{SC} values reported in this study using ENF specimens with shear precracks. However, the G_{Ic} value

extrapolated from the predominantly mode I EDT layup is lower than the G_{Ic} value in fig.19 that was measured from DCB tests. This difference is minimized if the influence of residual thermal stresses to G in the EDT test are included in the data reduction [8,25]; however, this would also increase the apparent G_{th} for this predominantly mode I case over the G_{IIth} measured in this study using the ENF test, which is difficult to rationalize physically. Because of the many variables that may influence toughness for the semicrystalline PEEK thermoplastic matrix composites, a detailed study should be conducted using a variety of tests on panels of this material as it is currently produced to fully characterize the toughness of AS4/PEEK.

Residual Static Tests

The degradation in residual G_{IIc} values for S2/SP250 laminates after 10^6 cycles (tables 8&9) indicates that matrix damage was created at the delamination front even though no coalescence occurred resulting in delamination growth. These data would suggest that delamination growth might occur at very long fatigue lives, perhaps on the order of 10^7 to 10^9 cycles. In some composite structures, such as helicopter rotor blades and hubs, these long lives are very common. Hence, for very long term durability, the G_{th} values measured at 10^6 cycles may be unconservative. Testing for delamination onset after 10^7 or more cycles is needed to confirm this perception. This long term testing may be very time consuming and costly. However, the flatness of the G_{max} versus cycles curves between 10^5 and 10^6 cycles (fig.14-18) suggests that G_{th} values will probably decrease very little beyond 10^6 cycles.

CONCLUSIONS

Based on the analysis and reduction of test data for the materials tested in this study, the following conclusions were reached:

1) Finite element analysis of the end-notched flexure (ENF) specimen indicates that the beam theory calculation for G_{II} with the transverse shear contribution included is reasonably accurate over the entire range of crack lengths. These G_{II}^{SH} values are slightly conservative compared to the finite element results, but the difference is minimal when the contribution of friction is included with the finite element results. Hence, G_{II}^{SH} values represent reasonably accurate calculations of the strain energy release rate associated with interlaminar shear in the ENF test.

2) ENF specimen compliance measurements, and the variation in compliance with delamination length, for the materials tested differed from the beam theory. This difference was attributed to the variation in ply thickness, and hence the variation in fiber volume fraction, through the thickness of the ENF specimens. For the materials tested in this study, the axial stiffness estimated from flexural tests was consistantly lower than values measured on the same ENF specimens in axial tension tests.

3) For the materials that exhibited linear load-deflection behavior in the ENF three-point bending test, G_{IIc} values determined from compliance

calibration measurements provided the most conservative and accurate estimate of interlaminar shear fracture toughness.

4) Cyclic loading significantly reduced the critical G_{II} for delamination onset. The maximum cyclic G_{II} level below which no delamination was observed after 10^6 cycles, i.e., the threshold cyclic G_{II} for delamination in fatigue, was determined for the three materials and was compared to the static G_{IIc} using the ENF test to quantify the degradation in interlaminar shear fracture toughness due to fatigue.

5) Toughened matrix materials, and brittle matrix materials that underwent low-load/high-cycle fatigue loading, exhibited nonlinear load-displacement behavior in the ENF test. For these cases, G_{II} calculated using the load at deviation from linearity may provide a more accurate and conservative estimate of the interlaminar shear fracture toughness.

6) Although a linear mixed-mode failure criterion is needed to characterize the static interlaminar fracture toughness of some composite materials, a total G threshold criterion appears to be sufficient for characterizing the fatigue delamination durability of composite laminates with a variety of static toughnesses.

ACKNOWLEDGEMENTS

The authors wish to acknowledge the contribution of Mr. Tracy Bridges of NASA Langley who designed and fabricated the three-point-bend fixture and

performed the static and fatigue tests in this study. The authors also wish to acknowledge the contribution and suggestions of Dr. I.S. Raju of Analytical Services and Materials, Inc. for the finite element analysis that was performed.

REFERENCES

[1] Abdallah, M.G.,"Review of the State of the Art of Advanced Composite Interlaminar Shear Test Methods", Proceedings of the 1986 SEM Spring Conference on Experimental Mechanics, New Orleans, La., June, 1986.

[2] Adams, D.O., and Kearney, H.L.,"Full-Scale Fatigue Testing of Advanced Fiber Composite Components", J. of the American Helicopter Society, Vol.31, No.2, April, 1986, p.66.

[3] Whitney, J.M., and Browning, C.E.,"On Short-Beam Shear Tests for Composite Materials", Experimental Mechanics, Vol.25, No.3, Sept. 1985, p.294.

[4] O'Brien, T.K.,"Interlaminar Fracture of Composites", J. of the Aeronautical Society of India, Vol. 37, No.1, Part III, p. 61, February 1985.

[5] O'Brien, T.K.,"Mixed-mode Strain-Energy-Release Rate Effects on Edge Delamination of Composites. Effects of Defects in Composite Materials, ASTM STP 836, 1984.

[6] O'Brien, T.K., "Generic Aspects of Delamination in Fatigue of Composite Materials," J. of the American Helicopter Society, Vol.32, No.1, January, 1987, p.13.

[7] Adams, D.F., Zimmerman, R.S., and Odem, E.M., "Determining Frequency and Load Ratio Effects on the Edge Delamination Test in Graphite Epoxy Composites," in Toughened Composites, ASTM STP 937, 1987.

[8] O'Brien, T.K., "Fatigue Delamination Behavior of PEEK Thermoplastic Composite Laminates", Proceedings of the American Society for Composites First Technical Conference, Dayton, Ohio, 1986, p.404.

[9] Russell, A.J., "On the Measurement of Mode II Interlaminar Fracture Energies," Defence Research Establishment Pacific (DREP) Canada, Materials Report 82-0, December, 1982.

[10] Russell, A.J., and Street, K.N.,"Moisture and Temperature Effects on the Mixed-mode Delamination Fracture of Unidirectional Graphite/Epoxy", Delamination and Debonding of Materials, ASTM STP 876, 1985, p.349.

[11] Russell, A.J., and Street, K.N., "Factors Affecting the Interlaminar Fracture Energy of Graphite/Epoxy Laminates", in Progress in Science and Engineering of Composites, Proceedings of the Fourth International Conference on Composite Materials (ICCM-IV), Tokyo, 1982, p.279.

[12] Murri, G.B.,and O'Brien, T.K., "Interlaminar G_{IIc} Evaluation of Toughened Resin Composites Using the End-notched Flexure Test," AIAA-85-0647, Proceedings of the 26th AIAA/ASME/ASCE/AHS Conference on Structures, Structural Dynamics, and Materials, Orlando, Florida, April, 1985, p.197.

[13] Mall, S., and Kochhar, N.K., "Finite Element Analysis of End Notched Flexure Specimens," J. of Composites Technology and Research, Vol.8, No.2, Summer 1986, p.54.

[14] Carlsson, L.A., Gillespie, J.W., and Pipes, R.B., "On the Analysis and Design of the End Notched Flexure (ENF) Specimen for Mode II Testing", J. of Composite Materials, Vol.20, November, 1986, p.594.

[15] Gillespie, J.W., Carlsson, L.A., and Pipes, R.B., "Finite Element Analysis of the End Notched Flexure Specimen for Measuring Mode II Fracture Toughness", Composites Science and Technology, Vol. 27, 1986, p.1.

[16] Carlsson, L.A., Gillespie, J.W., and Trethewey, B.R., "Mode II Interlaminar Fracture of Graphite/Epoxy and Graphite/PEEK", J. of Reinforced Plastics and Composites, Vol. 5, July, 1986, p.170.

[17] Carlsson, L.A., Gillespie, J.W., and Whitney, J.M., "Interlaminar Fracture Mechanics Analysis of the End Notched Flexure Specimen", Proceedings of the American Society for Composites First Technical Conference, Dayton, Ohio, 1986, p.421.

[18] Gillespie, J.W., Carlsson, L.A., Pipes, R.B., Rothschilds, R., Trethewey, B.R., and Smiley, A.J., "Delamination Growth in Composite Materials", NASA Contractor Report 178066, 1985.

[19] Smiley, A.J., and Pipes, R.B., "Rate Sensitivity of Interlaminar Fracture Toughness in Composite Materials", Proceedings of the American Society for Composites First Technical Conference, Dayton, Ohio, 1986, p.434.

[20] Trethewey, B.R., Carlsson, L.A., Gillespie, J.W., and Pipes, R.B., "Mode II Interlaminar Fracture During Static and Fatigue Loading", Center for Composite Materials Report CCM 86-26, University of Delaware, Newark, Delaware, Sept. 1986.

[21] Wakelyn, N.T., "Resolution of Wide Angle X-ray Scattering from a Thermoplastic Composite," J. of Polymer Science: Part A: Polymer Chemistry, Vol. 24, 1986, p.2101.

[22] Rybicki, E.F., Schmueser, D.W., and Fox, J., J. of Composite Materials, Vol. 11, 1977, p.470.

[23] Salpekar, S. A., Raju, I. S., and O'Brien, T. K., "Strain Energy Release Rate Analysis of the End-Notched Flexure Specimen using the Finite Element Method." NASA TM-100494, 1987.

[24] Johnson, W.S., and Mangalgiri, P.D., "Influence of the Resin on Mixed-mode Interlaminar Fracture," in Toughened Composites, ASTM STP 937, 1987.

[25] O'Brien, T.K., Johnston, N.J., Raju, I.S., Morris, D.H., and Simonds, R.A., "Comparisons of Various Configurations of the Edge Delamination Test for Interlaminar Fracture Toughness," in Toughened Composites, ASTM STP 937, 1987.

TABLE 1 - Material Properties

Material	E_{11}, Msi	E_{22}, Msi	G_{12}, Msi	ν_{12}	2h, in.	h^2E_{11}/G_{12}	V_f,%
S2/SP250	6.31	2.50	0.60	0.25	0.2270	0.1355	49.5
T300/BP907	17.11	1.20	0.83	0.29	0.1505	0.1167	56.3
AS4/PEEK	21.23	1.50	0.67	0.37	0.1243	0.1224	61.7

TABLE 2 - Compliance Calibration Data

$$C/C_0 = A_0 + A_3(a/L)^3$$

		Roller Fixture			Knife-Edge Fixture			Beam Theory	
Material	Spec.#	A_3	A_0	r^2	A_3	A_0	r^2	A_3	A_0
S2/SP250	255- 6	1.151	1.003	.999	1.226	1.000	.989	1.50	1.0
	255-17	1.230	.983	.990	1.408	1.000	.998		
	AVG.	1.191			1.317				
T300/BP907	0-2-11	1.313	1.012	.999	1.316	.991	.996	1.50	1.0
	0-2-9	1.296	1.036	.992	1.318	.994	.997		
	AVG.	1.305			1.317				
AS4/PEEK	3-20	1.446	.991	.991	1.801	1.007	.997	1.50	1.0
	3-19	1.482	1.002	.995	1.540	1.004	.997		
	AVG.	1.464			1.671				

TABLE 3 - Compliance Calibration Data

$$C_{SH}/C^{0}_{SH} = A_0 + A_1(a/L) + A_3(a/L)^3$$

Material	Spec.#	Roller Fixture A_3	Roller Fixture A_1	Roller Fixture A_0	Beam Theory & Shear A_3	Beam Theory & Shear A_1	Beam Theory & Shear A_0
S2/SP250	255- 6	1.140	.0113	1.000	1.399	0.839	1.000
	255-17	1.338	-.1199	1.014			
	AVG.	1.239	-.0543	1.007			
T300/BP907	0-2-11	1.259	.0606	0.996	1.412	0.847	1.000
	0-2-9	1.101	.2160	0.980			
	AVG.	1.180	.1383	0.988			
AS4/PEEK	3-20	1.527	-.0905	1.014	1.408	0.845	1.000
	3-19	1.511	-.0324	1.011			
	AVG.	1.519	-.0615	1.013			

TABLE 4 - Comparison of Measured Axial Moduli with Values from Flexural Compliance

Material	Spec.#	FX E_{11}, Msi Roller Fixture	FX E_{11}, Msi Knife-Edge Fixture	AX E_{11}, Msi Tension Test
S2/SP250	255- 6	5.42	5.95	5.83
	255-17	5.56	5.92	6.79
	AVG.	5.49	5.94	6.31
T300/BP907	0-2-11	12.44	13.38	17.25
	0-2-9	12.20	13.59	16.97
	AVG.	12.32	13.48	17.11
AS4/PEEK	3-20	15.76	15.64	22.76
	3-19	15.45	16.06	19.70
	AVG.	15.61	15.85	21.23

TABLE 5 - Difference in Measured and Calculated Axial Modulus

$$(E^{AX}_{11} - E^{FX}_{11}) / E^{AX}_{11}$$

Material	Roller Fixture	Knife-Edge Fixture
S2/SP250	0.130	0.059
T300/BP907	0.280	0.212
AS4/PEEK	0.265	0.253

TABLE 6 - Static ENF Data for T300/BP907

Spec.#	a, in.	C, in/lb	P_c,lbs.	C_0,in/lb	Fracture Toughness, in-lb/in^2 G_{IIc}^{BT}	G_{IIc}^{SH}	G_{IIc}^{CC}	G_{IIc}^{CCSH}	Pre-crack
1-2-3	0.80	1.67×10^{-4}	430	1.39×10^{-4}	10.73	11.13	9.56	9.50	shear
1-2-8	0.70	1.70×10^{-4}	420	1.50×10^{-4}	8.50	8.91	7.52	7.75	shear
1-2-9	0.80	1.88×10^{-4}	355	1.57×10^{-4}	8.23	8.54	7.33	7.29	ten.
0-2-8	1.00	2.04×10^{-4}	375	1.47×10^{-4}	13.24	13.55	12.00	11.45	none
0-2-6	1.10	1.71×10^{-4}	390	1.13×10^{-4}	13.18	13.44	12.04	11.39	none
1-2-5	0.80	1.70×10^{-4}	450	1.42×10^{-4}	11.97	12.40	10.66	10.59	none

TABLE 7 - Static ENF Data for AS4/PEEK

Spec.#	a, in.	C, in/lb	load, lbs. P_c	P_{NL}	Fracture Toughness, in-lb/in^2 G_{IIc}^{BT}	G_{IIc}^{SH}	G_{IIc}^{CC}	G_{IIc}^{CCSH}	G_{IIc}^{SC}	G_{IIc}^{SCSH}
3-6	0.65	2.94×10^{-4}	355	330	9.30	9.84	9.09	8.85	7.86	7.65
3-10	0.60*	2.25×10^{-4}	383	348	7.23	7.72	7.06	6.78	5.83	5.59
3-4	1.00	3.32×10^{-4}	335	295	17.20	17.62	16.89	17.16	13.10	13.31
3-4	0.85*	3.13×10^{-4}	356	310	15.01	15.52	14.71	14.79	11.15	11.21
3-12	1.10	2.95×10^{-4}	319	260	15.22	15.52	14.97	15.27	9.94	10.14
3-12	1.05	2.63×10^{-4}	355	315	16.09	16.44	15.81	16.10	12.45	12.68
3-12	1.00	2.54×10^{-4}	340	305	13.55	13.88	13.31	13.53	10.71	10.88
3-9	0.80	2.33×10^{-4}	615	255	30.63	31.80	30.00	29.99	5.16	5.16
3-7	0.60	2.42×10^{-4}	503	300	13.41	14.32	13.10	12.57	4.16	4.47
AVG.					15.29	15.85	14.99	15.00	8.98	9.01

* Cyclic Shear Precrack

TABLE 8 - Static ENF Data for S2/SP250

Spec.#	a, in.	C, in/lb	P_c,lbs.	C_0,in/lb	Fracture Toughness, in-lb/in^2 G_{IIc}^{BT}	G_{IIc}^{SH}	G_{IIc}^{CC}	G_{IIc}^{CCSH}
255-20	0.85	1.60×10^{-4}	306	1.31×10^{-4}	5.66	5.87	4.76	4.95
255-20	0.90	1.42×10^{-4}	363	1.13×10^{-4}	7.64	7.89	6.38	6.66
255-20	0.95	1.46×10^{-4}	357	1.12×10^{-4}	8.09	8.33	6.81	7.08
255-18	0.60	1.18×10^{-4}	680	1.10×10^{-4}	11.99	12.89	9.69	10.80
255-17	0.60	1.25×10^{-4}	505	1.16×10^{-4}	6.98	7.51	5.64	6.31
255-6	0.60	1.19×10^{-4}	530	1.11×10^{-4}	7.31	7.86	5.91	6.62
255-19	0.60	1.21×10^{-4}	510	1.12×10^{-4}	6.89	7.40	5.56	6.23
255-10	0.60	1.20×10^{-4}	522	1.12×10^{-4}	7.16	7.70	5.78	6.47
255-3	0.60	1.20×10^{-4}	496	1.12×10^{-4}	6.47	6.95	5.22	5.84
AVG.					7.58	8.05	6.19	6.77

TABLE 9 - Residual Static ENF Data for S2/SP250

Spec.#	a, in.	C, in/lb	load, lbs. P_c	P_{NL}	Fracture Toughness, in-lb/in^2 G_{IIc}^{BT}	G_{IIc}^{SH}	G_{IIc}^{CC}	G_{IIc}^{CCSH}	G_{IIc}^{SC}	G_{IIc}^{SCSH}
255-8	0.90	1.44×10^{-4}	340	270	6.79	7.02	5.67	5.93	3.58	3.74
255-16	0.90	1.28×10^{-4}	372	255	7.22	7.42	6.04	6.31	2.84	2.96
255-4	0.65	1.37×10^{-4}	366	300	4.61	4.90	3.74	4.11	2.51	2.76
255-9	0.70	1.33×10^{-4}	365	300	5.02	5.30	4.10	4.44	2.77	3.00
AVG.					5.91	6.16	4.89	5.20	2.92	3.12

TABLE 10 - Fatigue ENF Data for T300/BP907

Spec.#	a, in.	C, in/lb	P_{max},lb.	G_{IImax}, in-lb/in^2				Cycles,N
				G_{II}^{BT}	G_{II}^{SH}	G_{II}^{CC}	G_{II}^{CCSH}	
0-4-9	1.08	2.00×10^{-4}	250	6.23	6.36	5.68	5.38	280
0-4-8	0.75	1.71×10^{-4}	260	3.65	3.80	3.24	3.27	490
0-4-4	0.95	1.71×10^{-4}	200	2.98	3.06	2.69	2.58	10,140
0-4-2	1.18	2.20×10^{-4}	150	2.66	2.70	2.44	2.30	1,745
0-4-3	0.90	2.00×10^{-4}	170	2.36	2.43	2.12	2.05	7,900
0-4-7	0.85	1.70×10^{-4}	170	1.86	1.92	1.67	1.63	18,830
0-2-5	0.97	2.10×10^{-4}	130	1.58	1.62	1.43	1.37	23,400
0-4-11	0.65	2.00×10^{-4}	160	1.29	1.36	1.13	1.20	28,100
0-2-6	0.80	1.80×10^{-4}	140	1.23	1.27	1.09	1.09	37,240
0-2-11	1.00	2.00×10^{-4}	110	1.12	1.14	1.01	0.97	331,850
0-2-8	1.00	2.12×10^{-4}	100	0.98	1.00	0.89	0.85	562,200
0-2-9	0.90	2.25×10^{-4}	90	0.74	0.77	0.67	0.65	>1,000,000

TABLE 11 - Fatigue ENF Data for S2/SP250

Spec.#	a, in.	C, in/lb	P_{max},lb.	G_{IImax}, in-lb/in^2				Cycles,N
				G_{II}^{BT}	G_{II}^{SH}	G_{II}^{CC}	G_{II}^{CCSH}	
255-15	1.00	1.50×10^{-4}	150	1.56	1.60	1.32	1.36	13,500
255-15	0.95	1.52×10^{-4}	150	1.49	1.54	1.25	1.30	16,800
255-14	0.90	1.42×10^{-4}	170	1.67	1.72	1.40	1.46	19,000
255-11	0.60	1.18×10^{-4}	244	1.53	1.65	1.50	1.39	300,000
255-8	0.90	1.41×10^{-4}	160	1.47	1.52	1.23	1.29	>1,000,000
255-2	0.90	1.50×10^{-4}	160	1.57	1.61	1.31	1.37	>1,000,000
255-16	0.90	1.43×10^{-4}	150	1.31	1.36	1.10	1.15	>1,000,000
255-4	0.65	1.29×10^{-4}	150	0.73	0.78	0.59	0.65	>1,088,000
255-7	0.80	1.33×10^{-4}	140	0.91	0.94	0.75	0.79	>1,000,000
255-9	0.70	1.48×10^{-4}	145	0.88	0.93	0.72	0.78	>1,550,000

TABLE 12 - Fatigue ENF Data for AS4/PEEK

Spec.#	a, in.	C, in/lb	P_{max},lb.	G_{IImax}, in-lb/in^2				Cycles,N
				G_{II}^{BT}	G_{II}^{SH}	G_{II}^{CC}	G_{II}^{CCSH}	
3-22	0.60	2.35×10^{-4}	332	5.68	6.07	5.55	5.32	580
3-15	0.60	2.34×10^{-4}	257	3.39	3.62	3.31	3.17	3,250
3-17	0.60	2.29×10^{-4}	182	1.66	1.77	1.62	1.56	30,000
3-11	0.60	2.33×10^{-4}	133	0.90	0.97	0.88	0.85	144,000
3-13	0.60	2.25×10^{-4}	125	0.77	0.82	0.75	0.72	>1,000,000

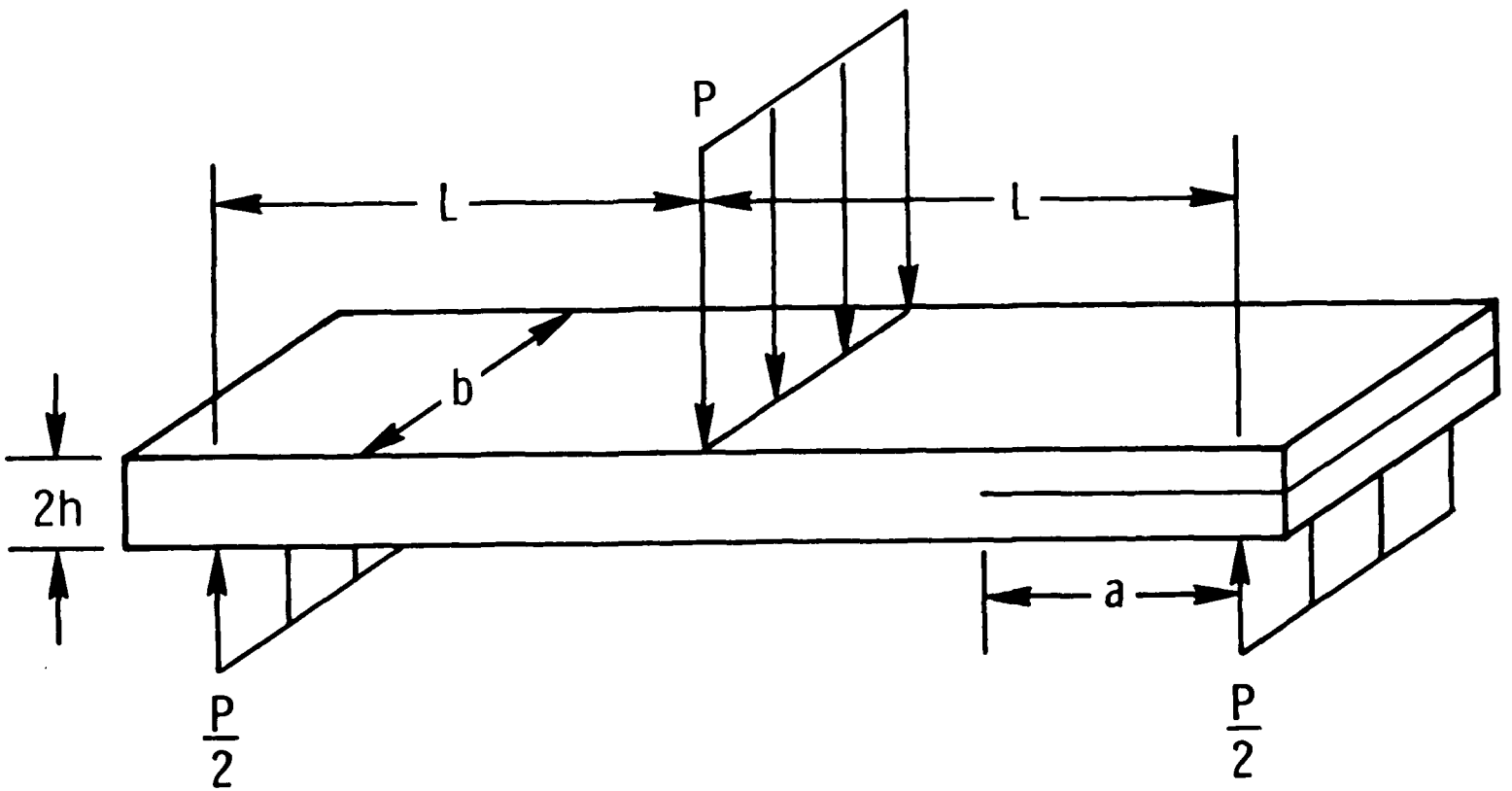

Fig. 1. Diagram of ENF specimen

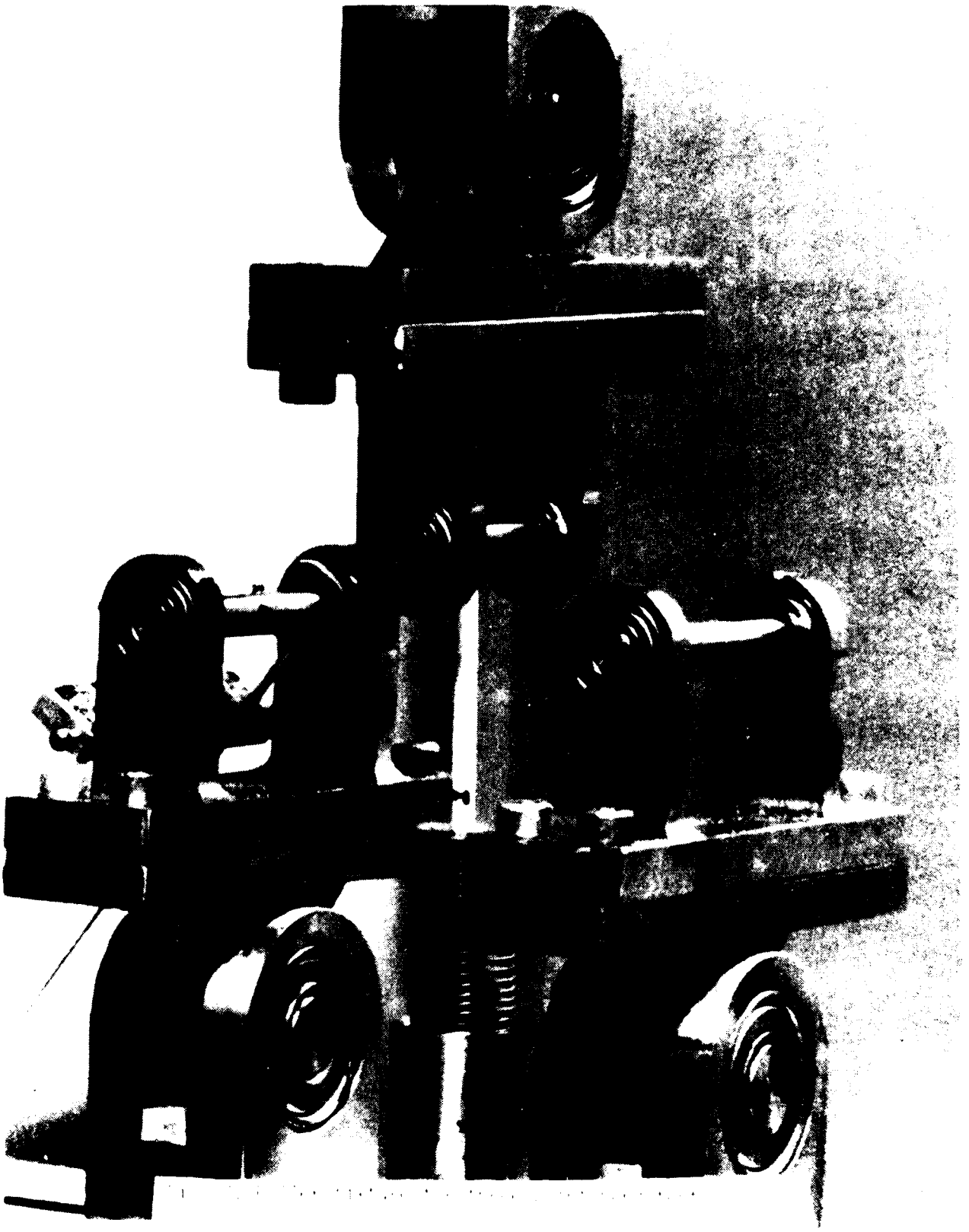

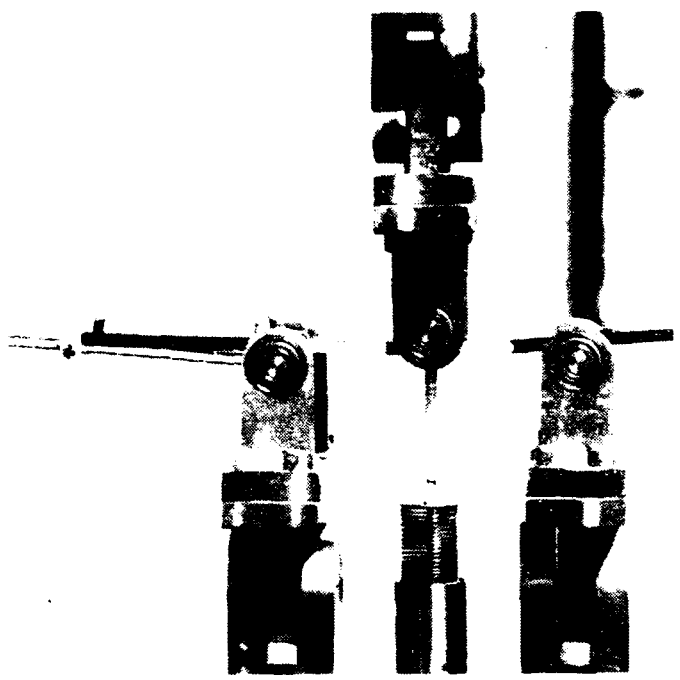

Graphite thermoplastic

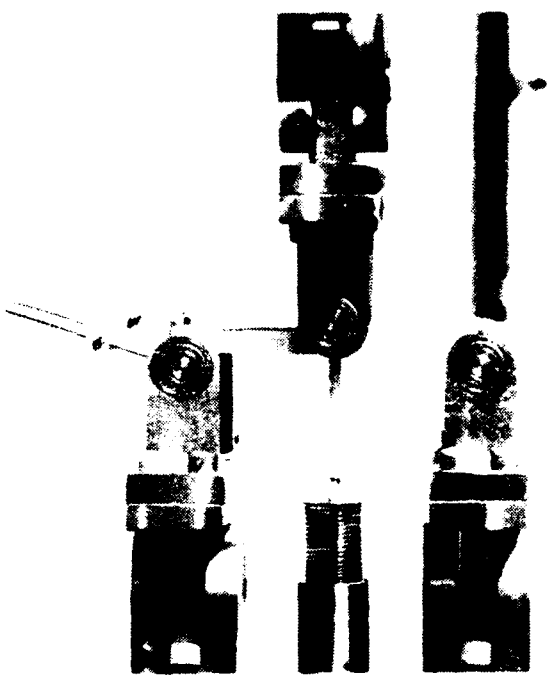

Glass epoxy

. . . . . loaded in the test fixture

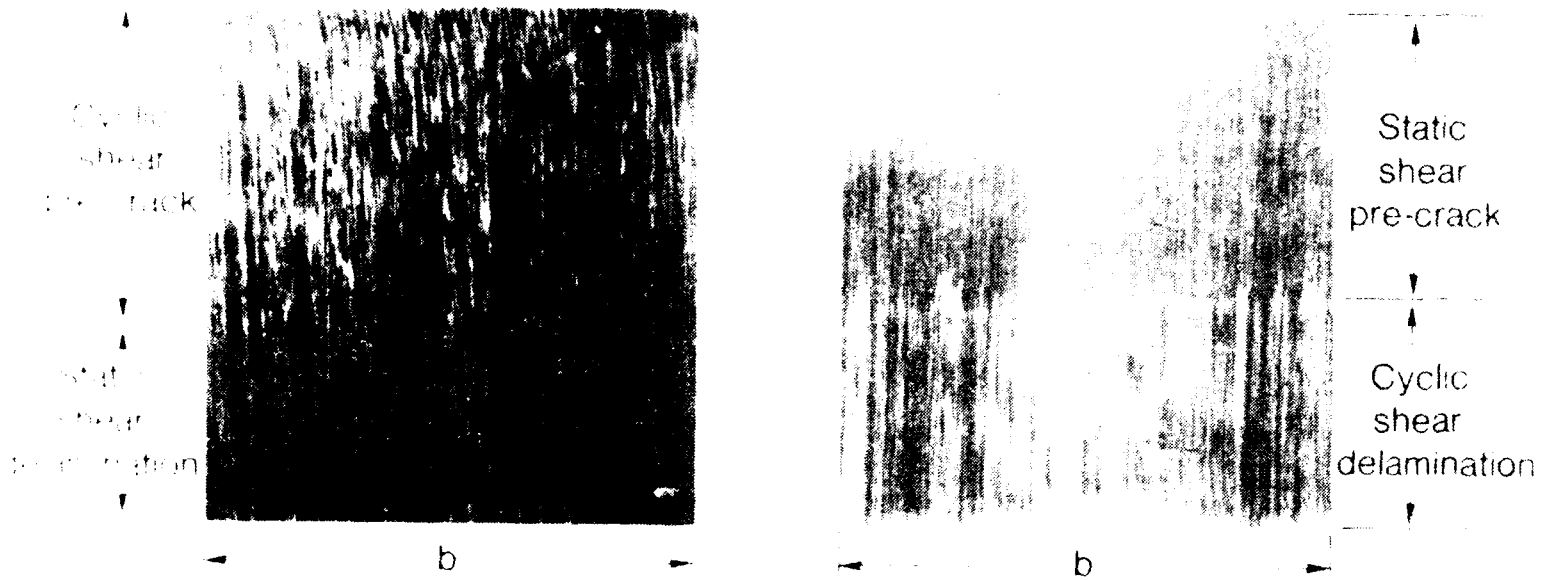

[illegible] difference in static and fatigue fracture surfaces for [illegible]

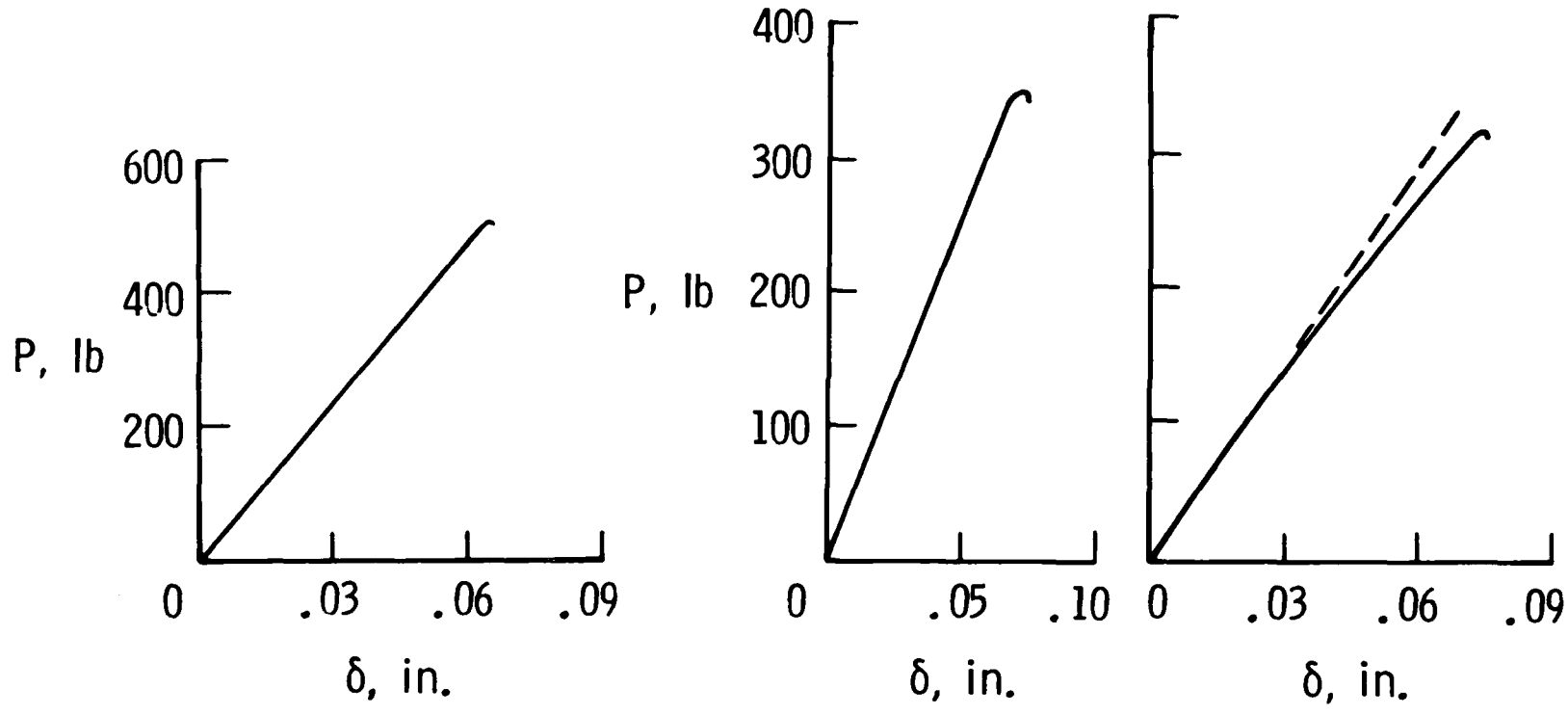

Fig. 5. Typical ENF load-displacement plots

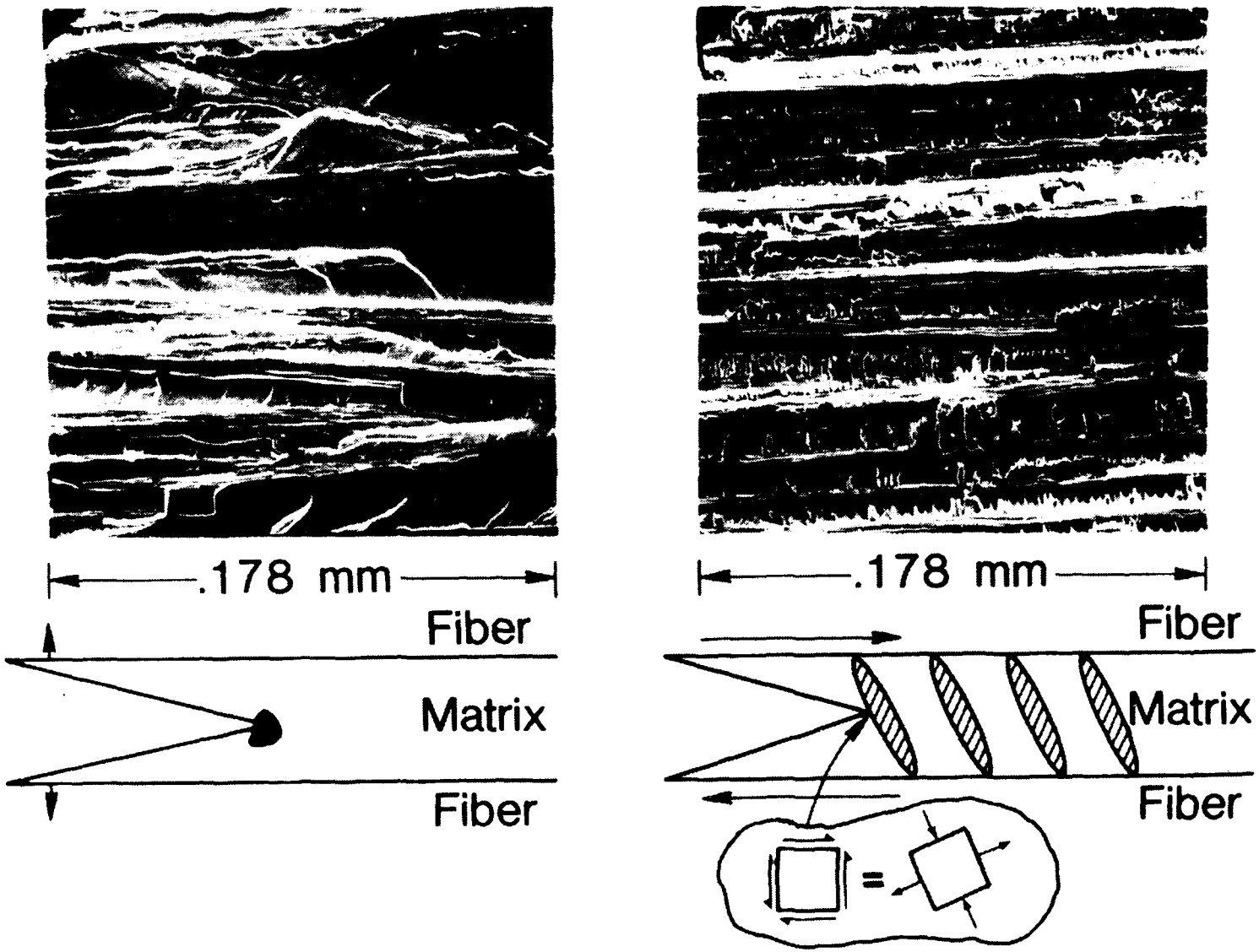

Fig. 6. Fracture surfaces of brittle (5208) material

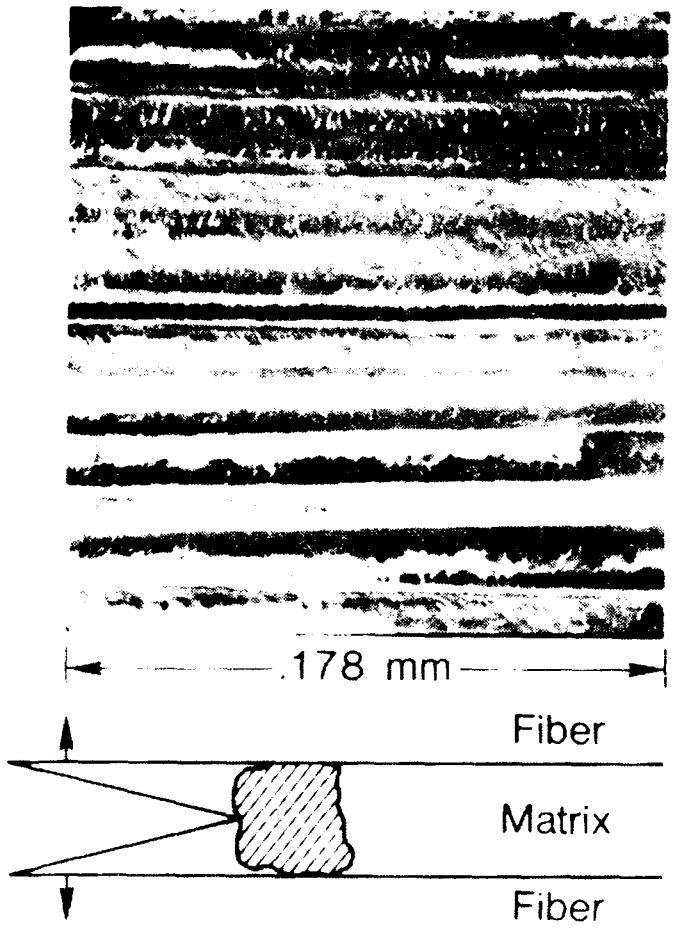
.178 mm
Fiber
Matrix
Fiber

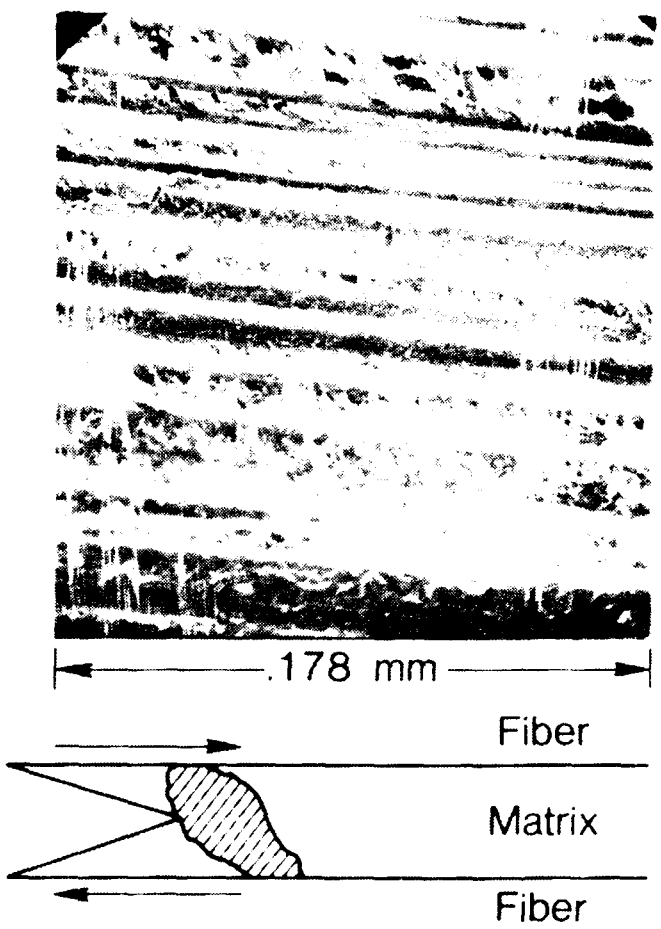
.178 mm
Fiber
Matrix
Fiber

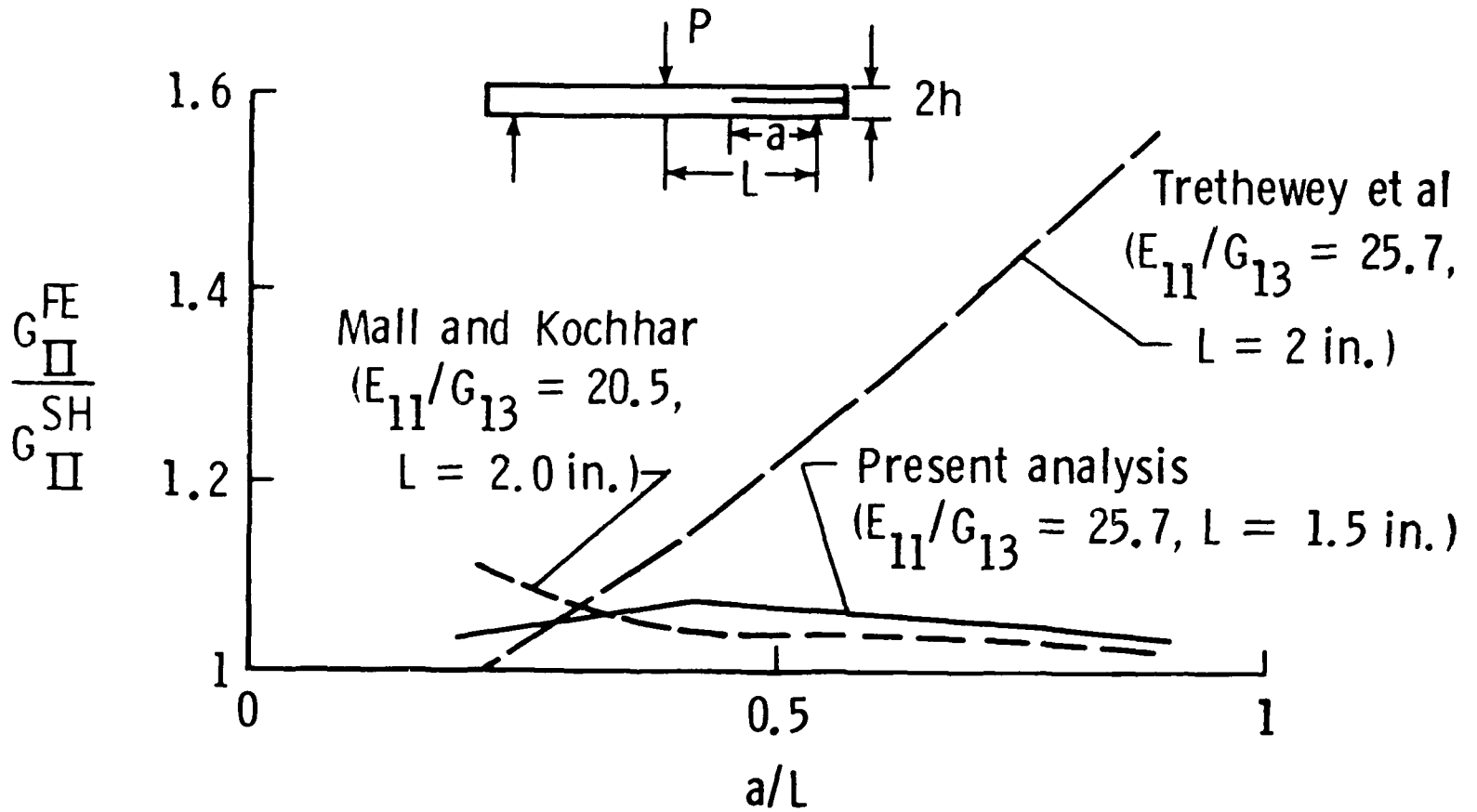

Fig. 8. Comparison of G_{II} from various analyses

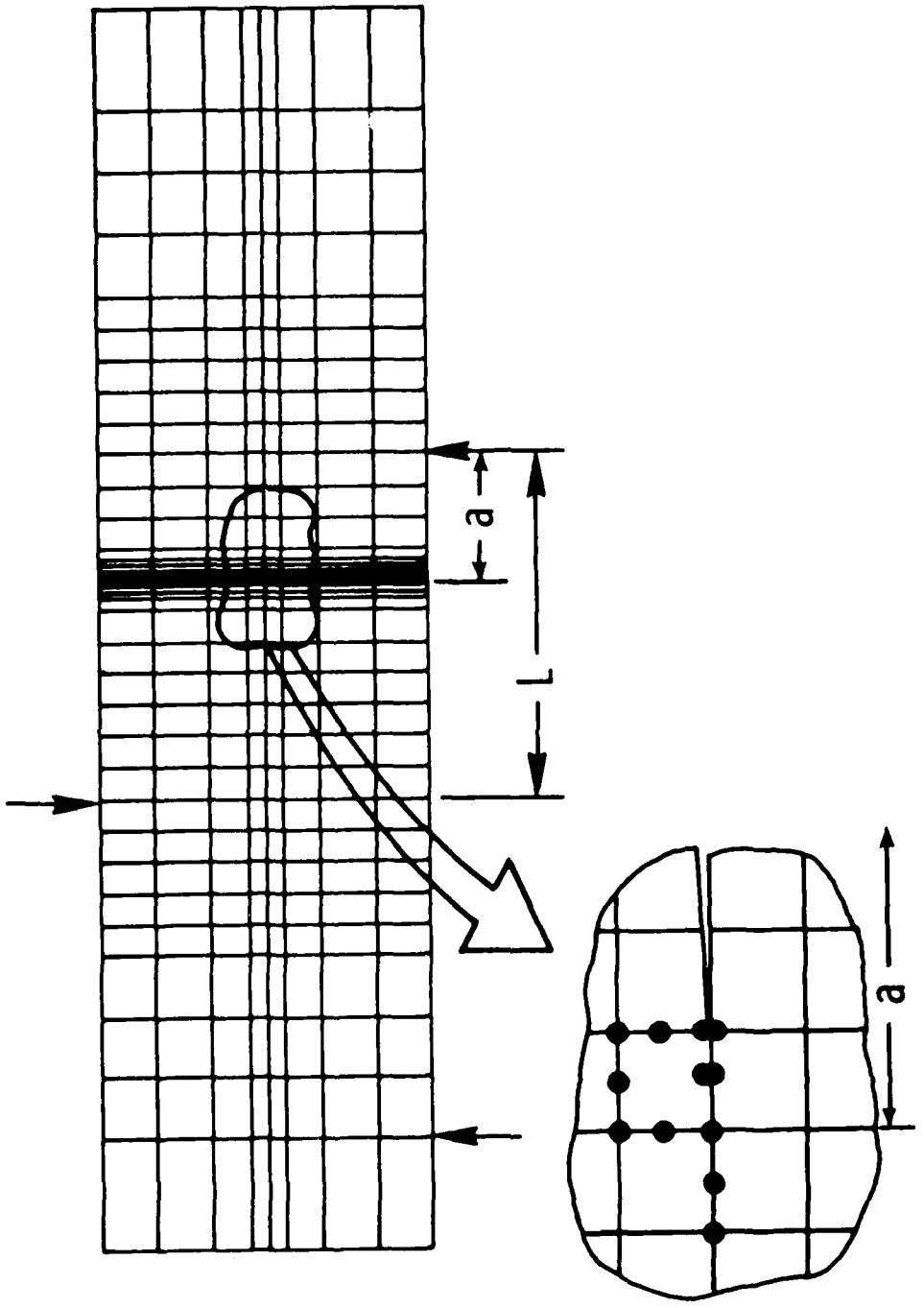

Fig. 9. Finite-element mesh for the ENF specimen

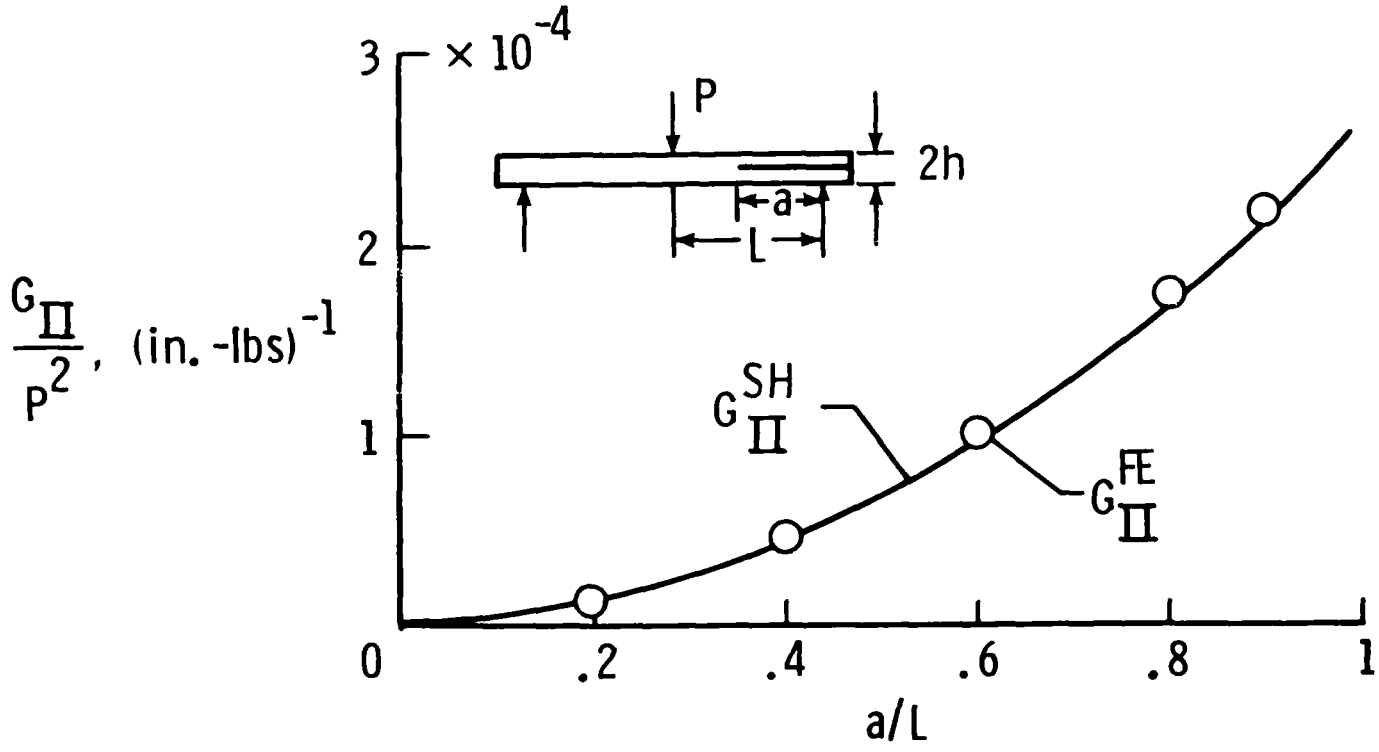

Fig.10. Normalized mode II strain energy release rate as a function of delamination length in the ENF test

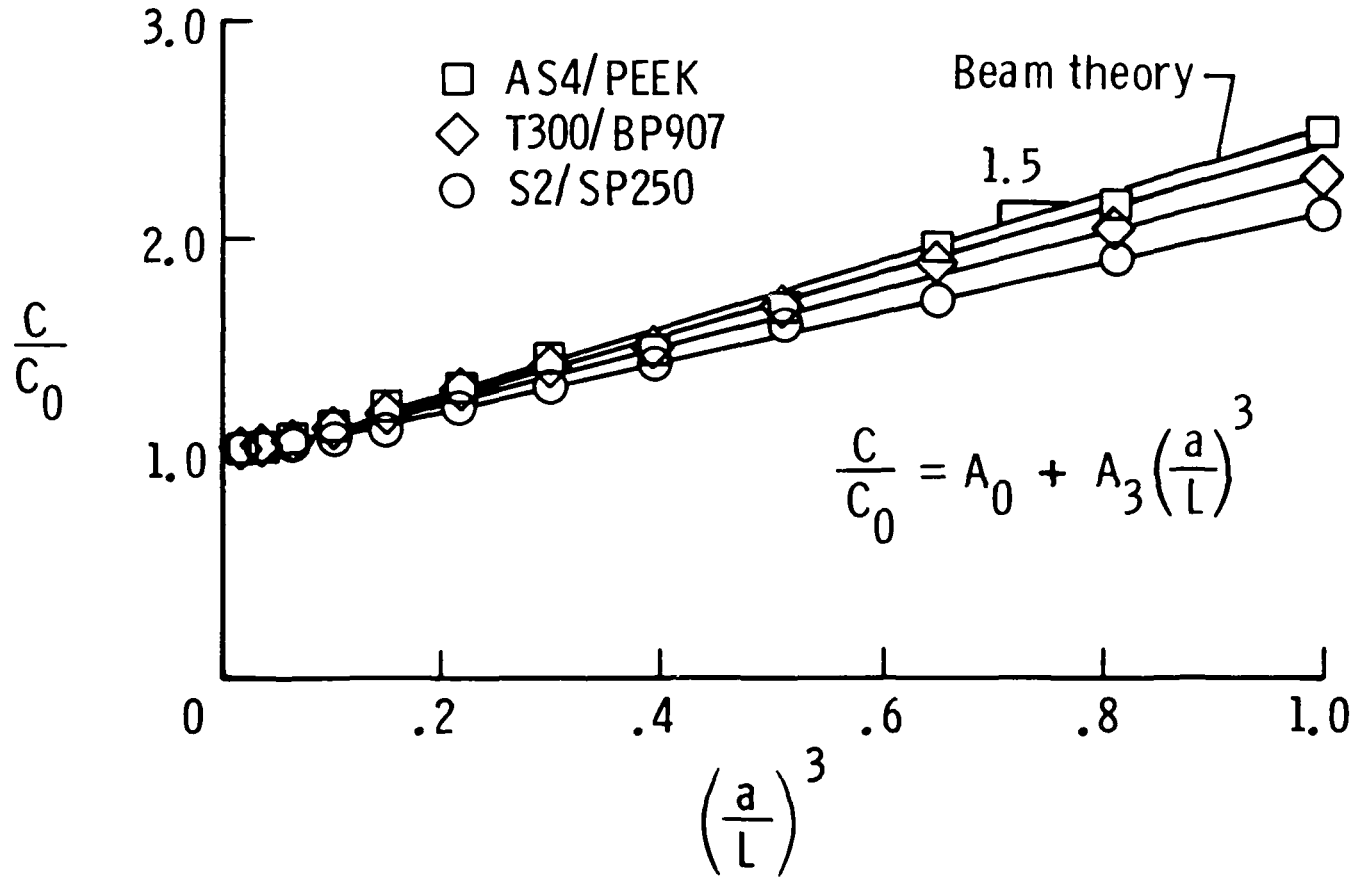

Fig.11. Linear regression analysis of compliance calibration data

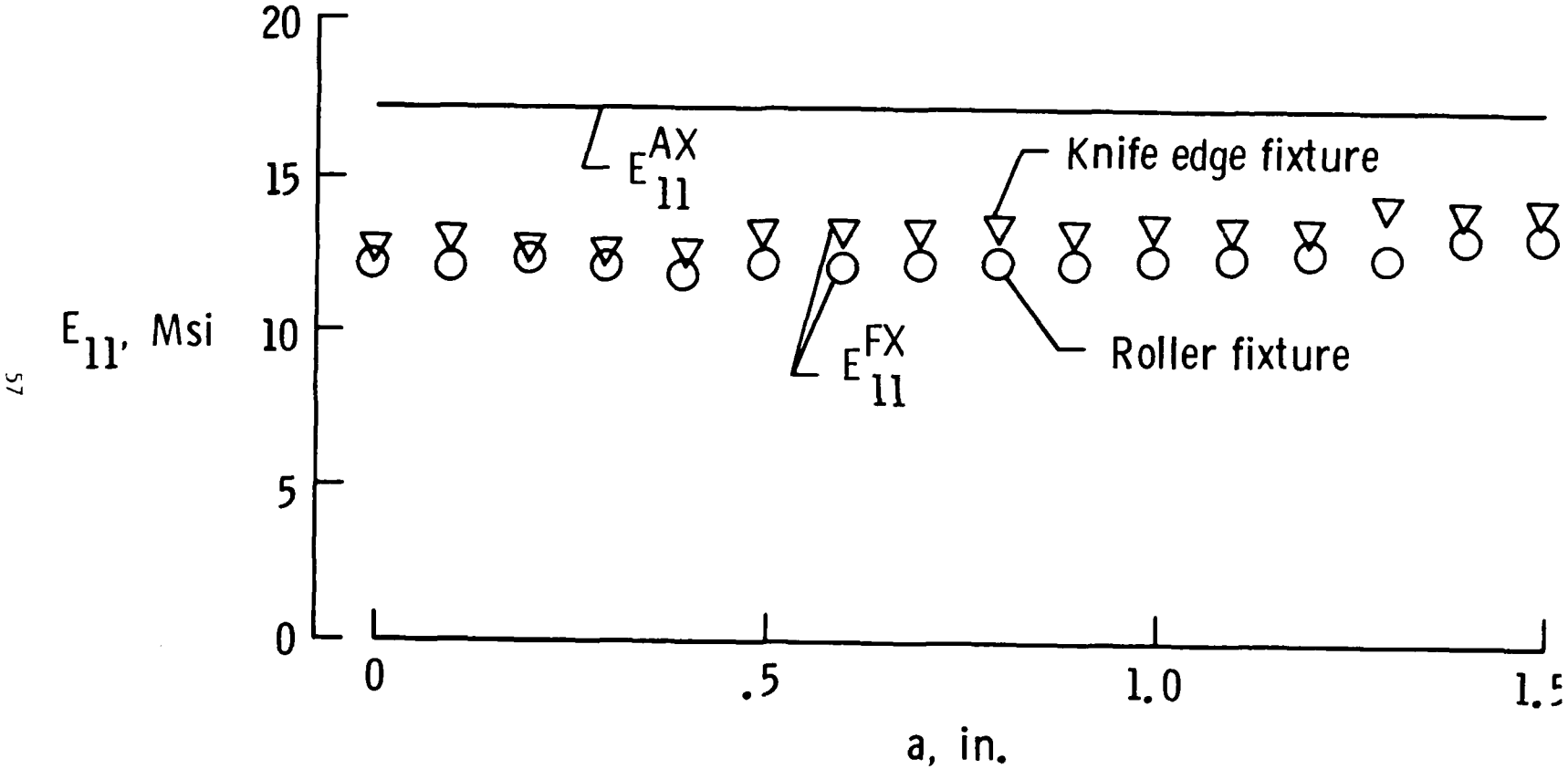

Fig.12. Axial stiffness comparison for T300/BP907

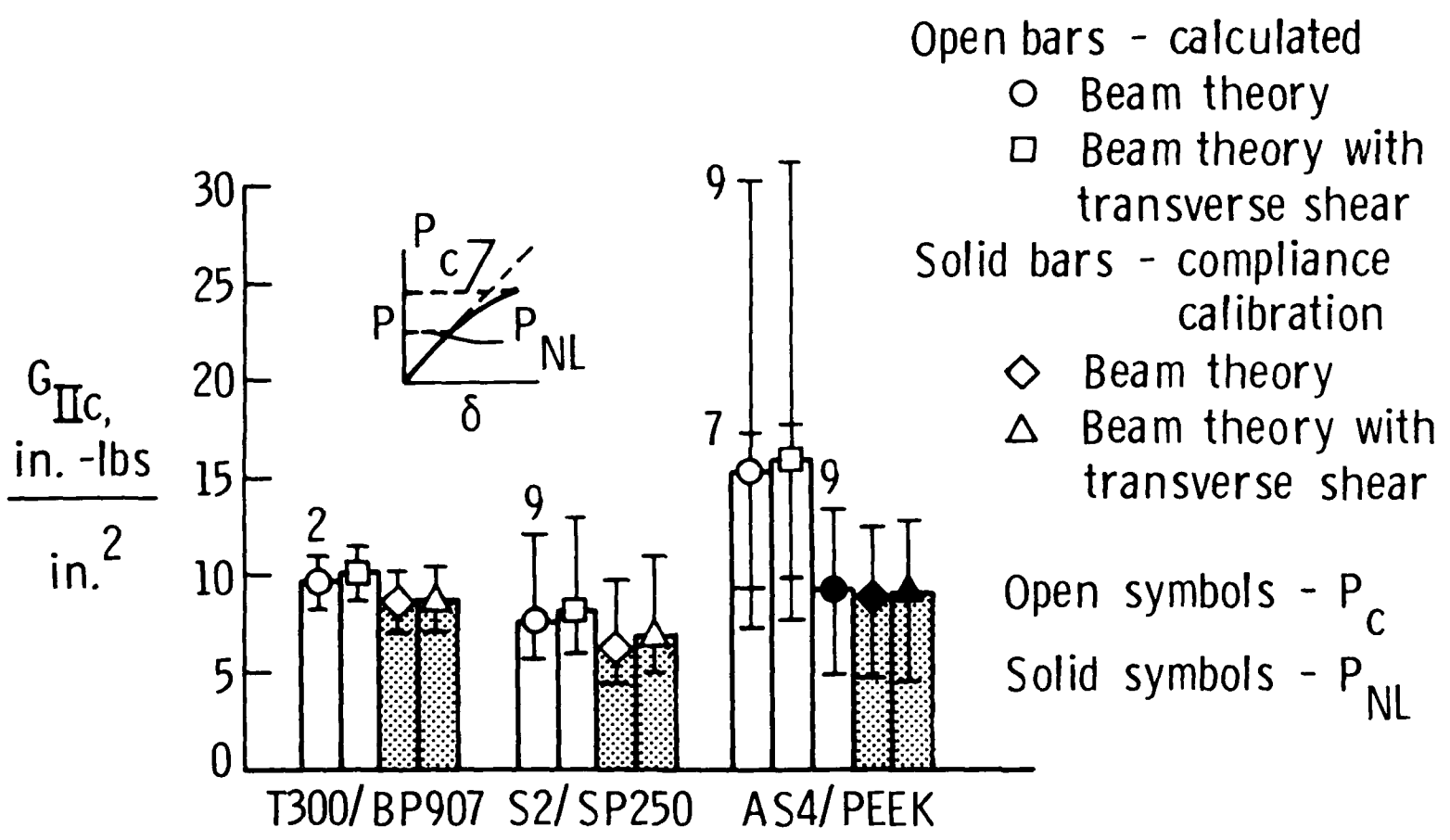

Fig.13. Interlaminar fracture toughness from the ENF test

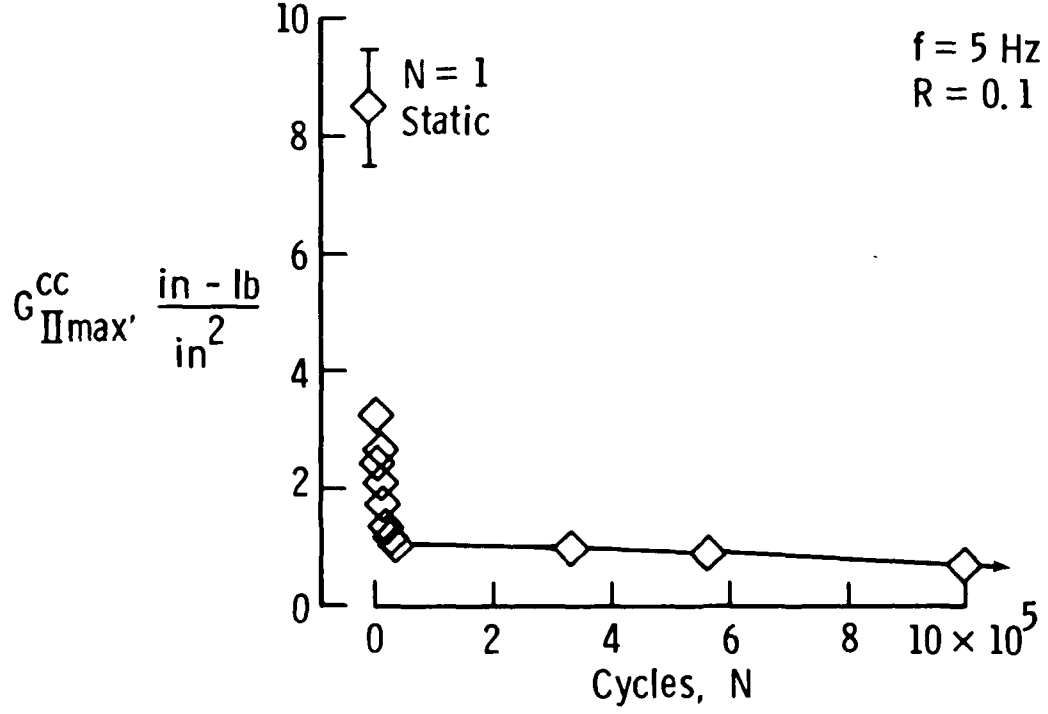

Fig.14. G^{CC}_{IImax} as a function of cycles to delamination onset for T300/BP907

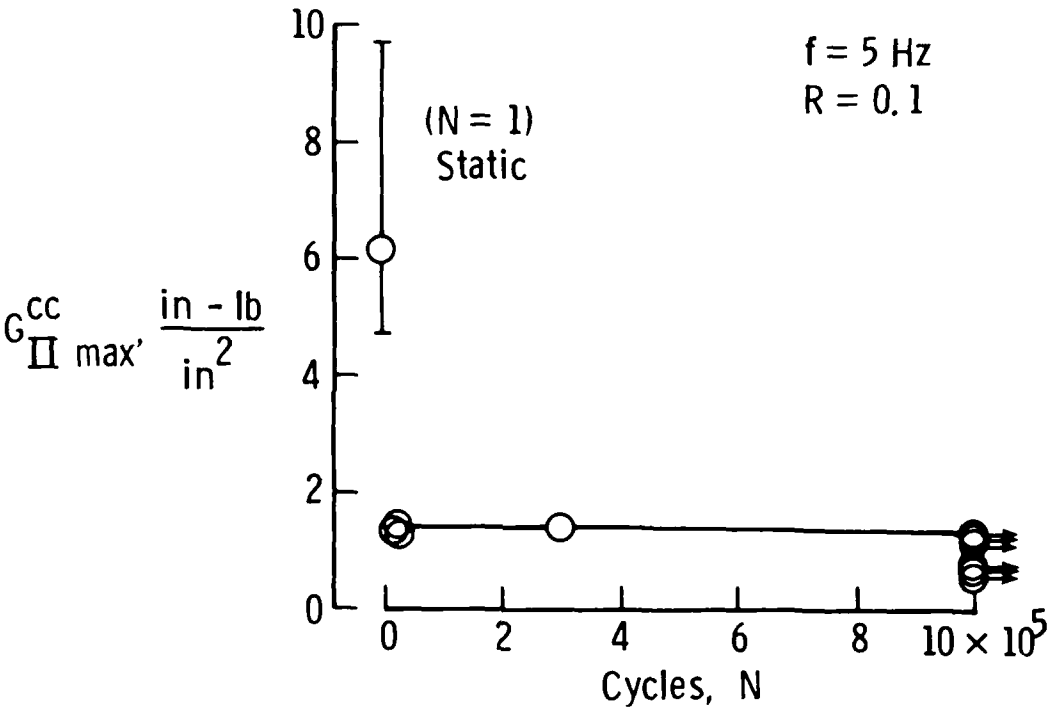

Fig.15. G^{CC}_{IImax} as a function of cycles to delamination onset for S2/SP250

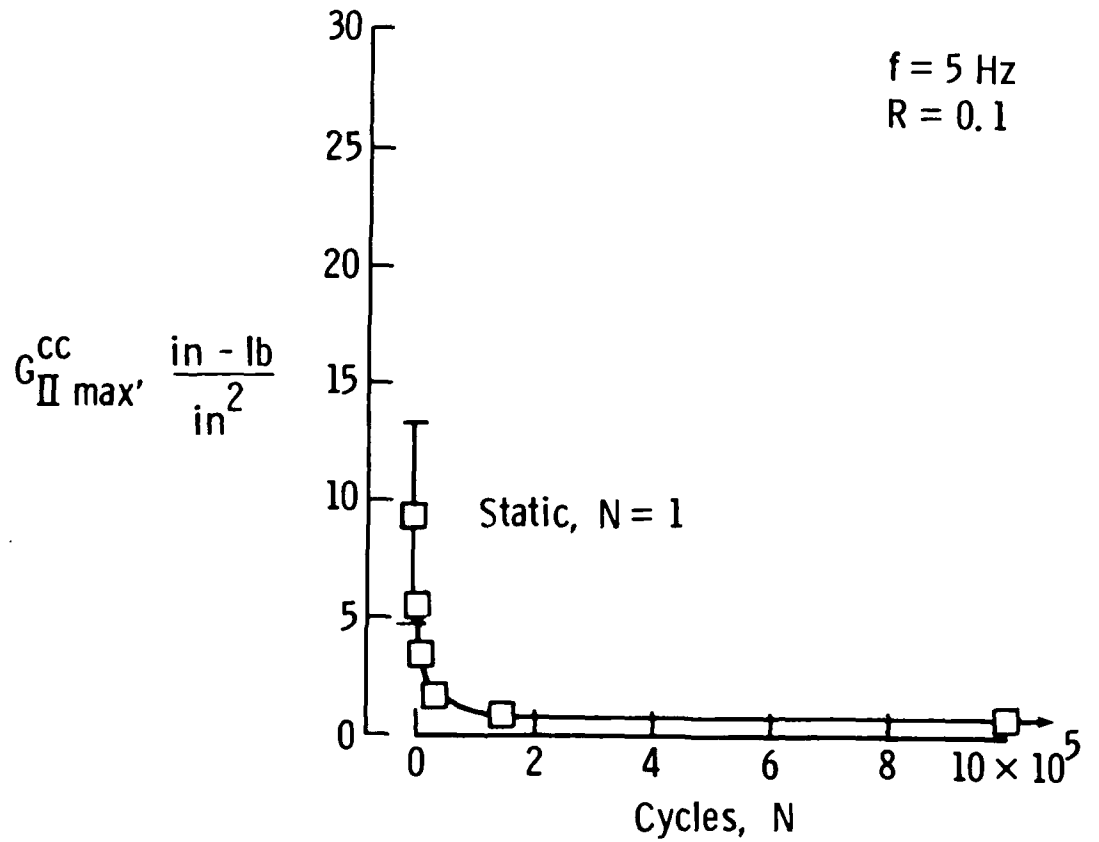

Fig.16. G_{IImax}^{CC} as a function of cycles to delamination onset for AS4/PEEK

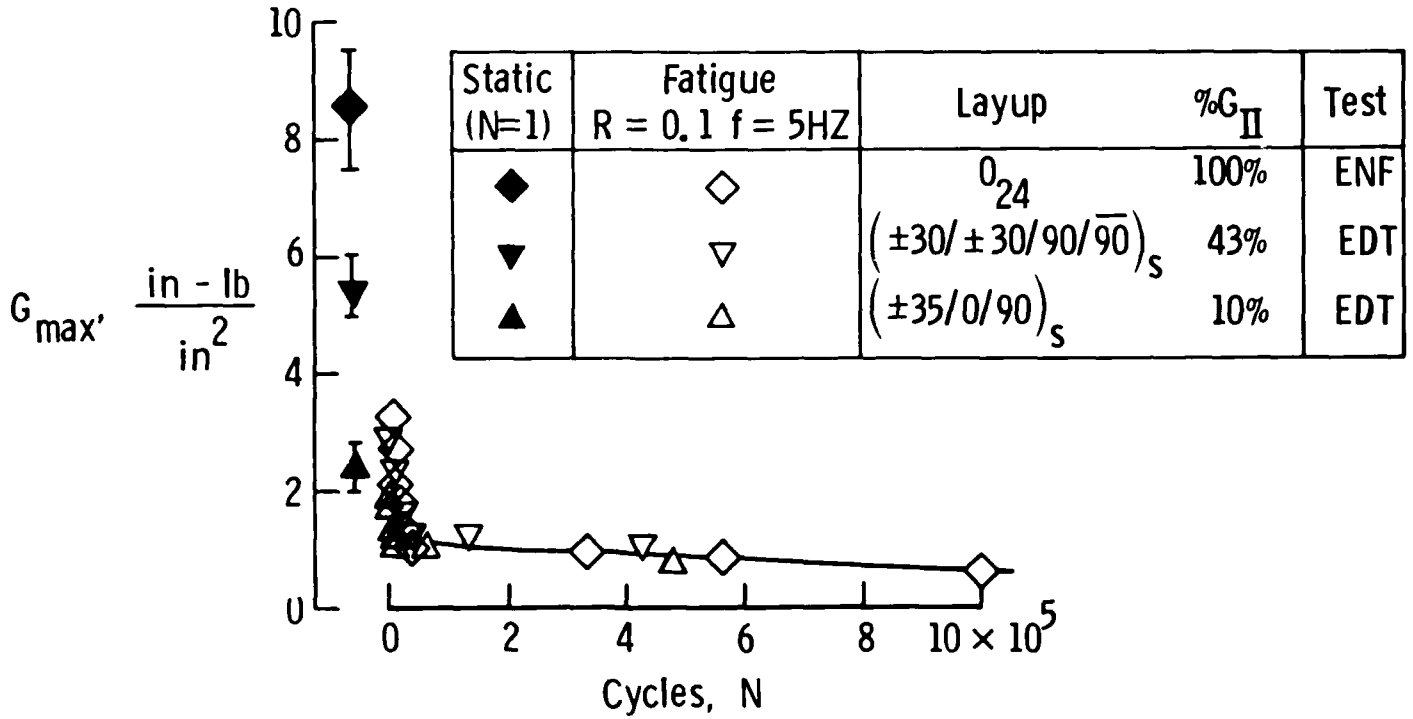

Fig.17. Comparison of static G_c and fatigue G_{th} values for delamination onset for T300/BP907 EDT and ENF tests

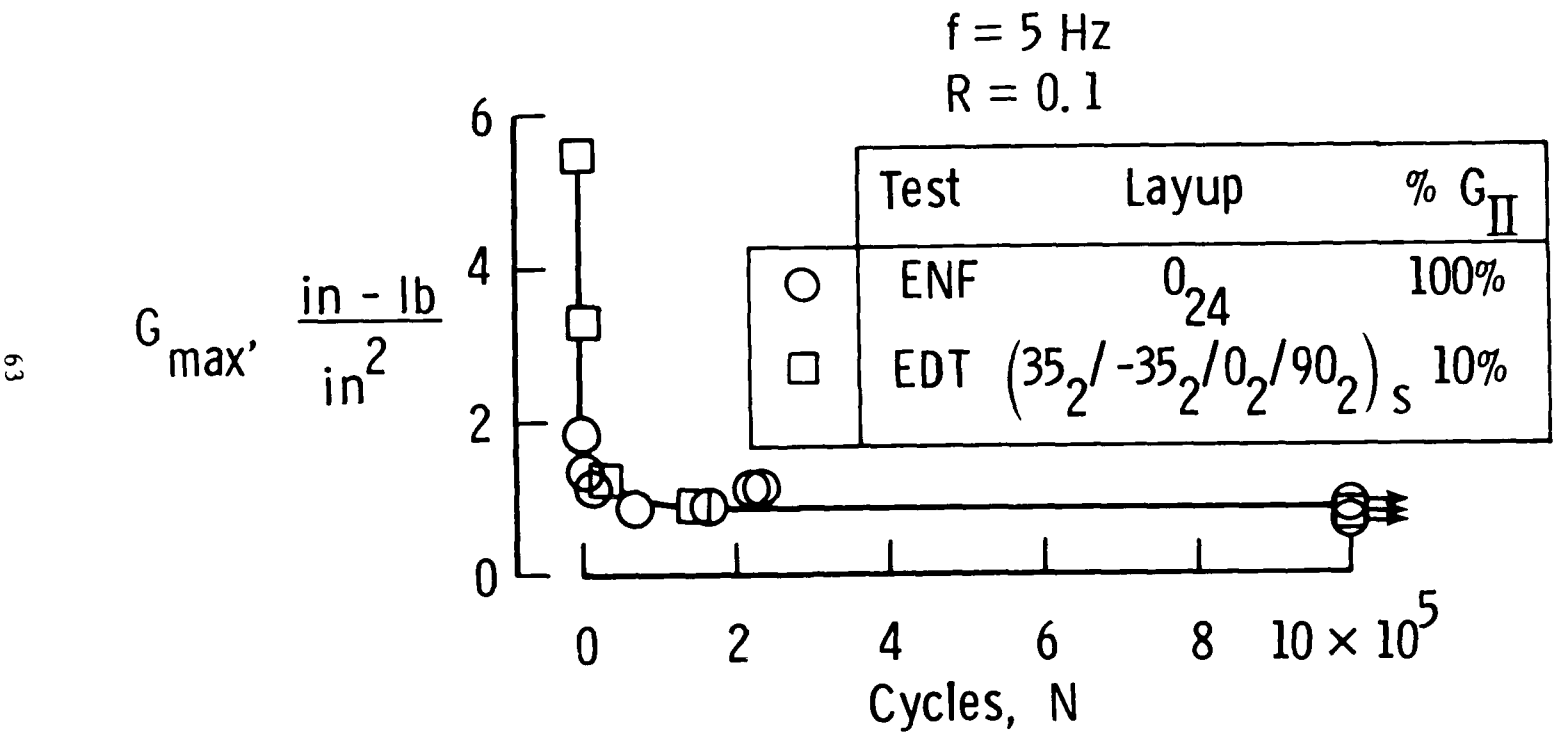

Fig.18. Maximum cyclic G as a function of cycles to delamination onset for AS4/PEEK EDT and ENF tests

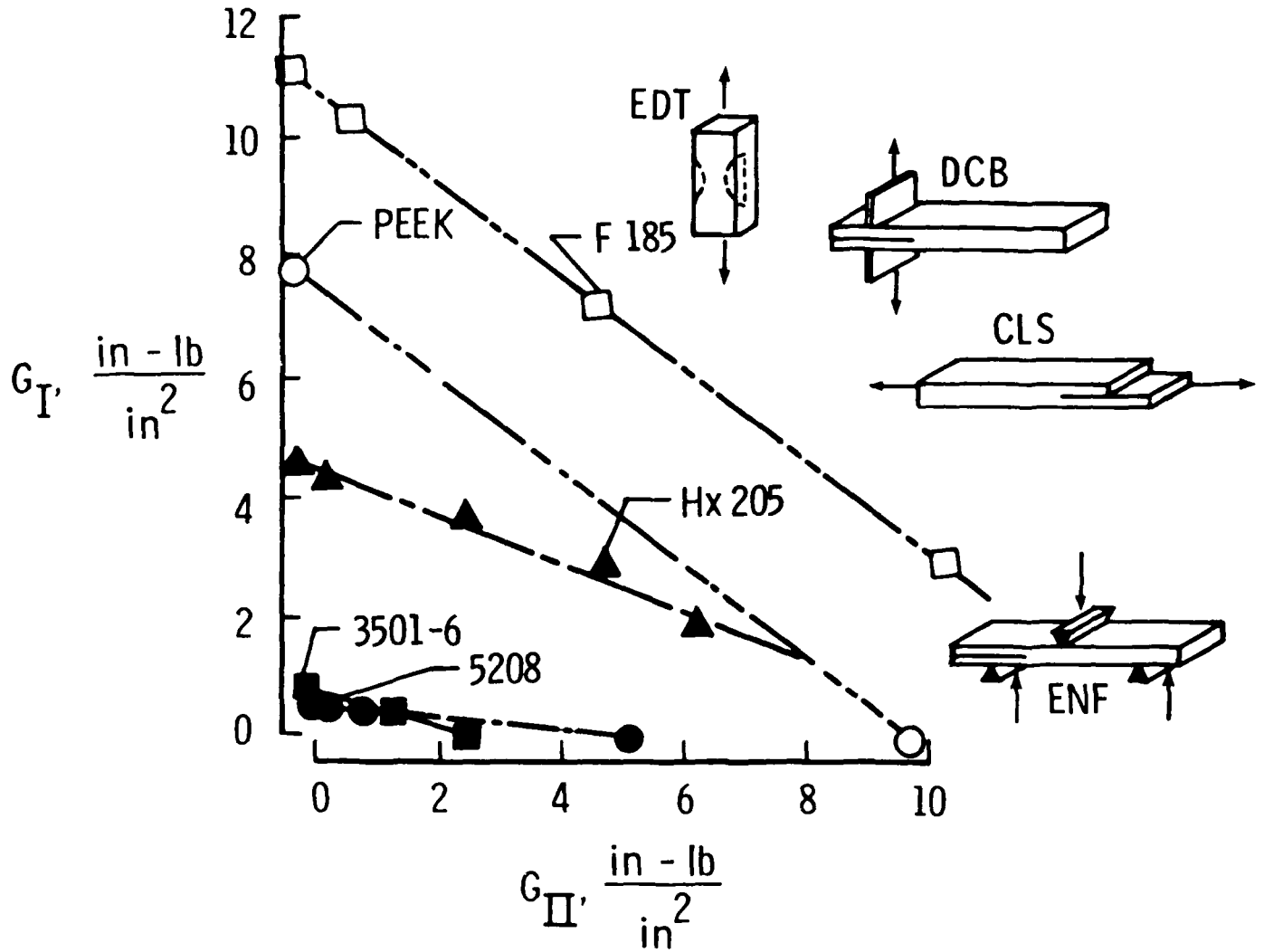

Fig.19. Mixed-mode fracture toughness

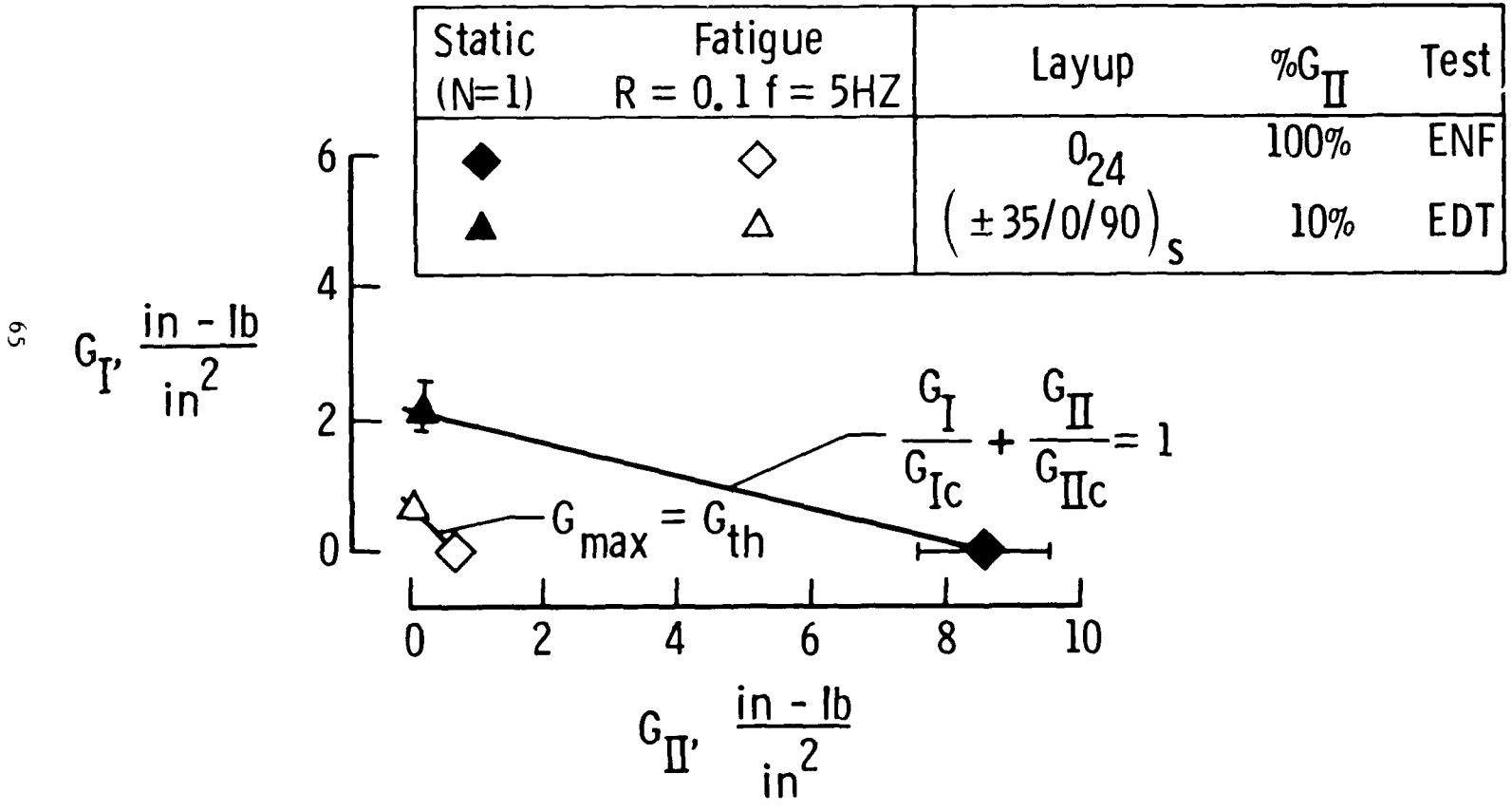

Fig.20 Mixed-mode fracture toughness and fatigue threshold criteria for T300/BP907

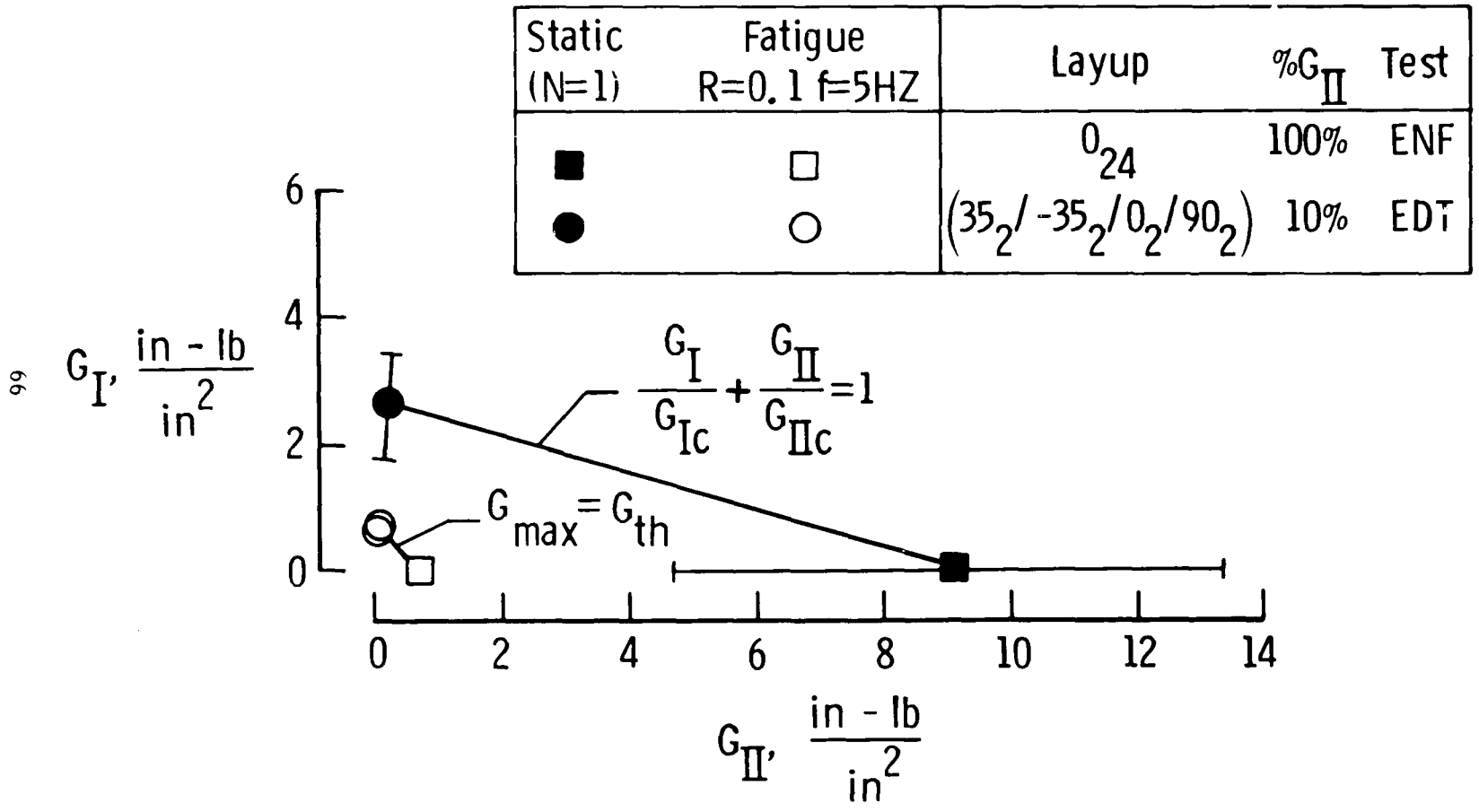

Fig.21. Mixed-mode fracture toughness and fatigue threshold criteria for AS4/PEEK

END

12-87

DTIC